Remote Sensing of Environment xxx (2015) xxx–xxx

Contents lists available at ScienceDirect

Remote Sensing of Environment

journal homepage: www.elsevier.com/locate/rse

Modeling grassland spring onset across the Western United States using climate variables and MODIS-derived phenology metrics

Qinchuan Xin [a,*], Mark Broich [b], Peng Zhu [a], Peng Gong [a,c,d]

[a] Ministry of Education Key Laboratory for Earth System Modeling, Tsinghua University, Beijing, China
[b] School of Biological, Earth and Environmental Sciences, University of New South Wales, Sydney, Australia
[c] Environmental Science, Policy and Management and Geography, University of California, Berkeley, CA, USA
[d] Joint Center for Global Change Studies, Beijing, China

ARTICLE INFO

Article history:
Received 23 July 2014
Received in revised form 3 February 2015
Accepted 3 February 2015
Available online xxxx

Keywords:
Remote sensing
Phenology model
Flux tower
Climate variability

ABSTRACT

Vegetation phenology strongly controls photosynthetic activity and ecosystem function and is essential for monitoring the response of vegetation to climate change and variability. Terrestrial ecosystem models require robust phenology models to understand and simulate the relationship between ecosystems and a changing climate. While current phenology models are able to capture inter-annual variation in the timing of vegetation spring onset, their spatiotemporal performances are not well understood. Using green-up dates derived from MODIS, we test 9 phenological models that predict the timing of grassland spring onset via commonly available climatological variables. Model evaluation using satellite observations suggests that Modified Growing-Degree Day (MGDD) models and Accumulated Growing Season Index (AGSI) models achieve reasonable accuracy (RMSE < 20 days) after model calibration. Inclusion of a photoperiod trigger and varied critical forcing thresholds in the temperature-based phenology model improves model applicability at a regional scale. In addition, we observe that AGSI models outperform MGDD models by capturing inter-annual phenology variation in large semi-arid areas, likely due to the explicit consideration of water availability. Further validation based on flux tower sites shows good agreement between the modeled timing of spring onset and references derived from satellite observations and in-situ measurements. Our results confirm recent studies and indicate that there is a need to calibrate current phenology models to predict grassland spring onsets accurately across space and time. We demonstrate the feasibility of combining satellite observations and climatic datasets to develop and refine phenology models for characterizing the spatiotemporal patterns of grassland green-up variations.

1. Introduction

Vegetation phenology, characterizing the recurring and periodic cycles of vegetation green-up and senescence, is highly sensitive to climate change and variability (Cleland, Chuine, Menzel, Mooney, & Schwartz, 2007; Koerner & Basler, 2010; Piao, Fang, Zhou, Ciais, & Zhu, 2006; Richardson et al., 2013). Environmental drivers, such as temperature, photoperiod, water and nutrient availability, regulate the timing of the spring onset of natural vegetation (Friedl et al., 2014; Piao et al., 2011; Yu, Price, Ellis, & Shi, 2003). Numerous studies using in-situ measurements and satellite observations have documented decadal shifts in vegetation phenology under a changing climate at both regional and global scales (Broich et al., 2014; Julien & Sobrino, 2009; Wu & Liu, 2013; Yang, Mustard, Tang, & Xu, 2012). The shifts of key phenophases, such as spring onset and autumn senescence, control vegetation photosynthetic activities (Churkina, Schimel, Braswell, & Xiao, 2005; Richardson et al., 2010) and have profound impacts on global carbon and water cycles in both field measurements and model simulations (Dragoni et al., 2011; Jeong, Medvigy, Shevliakova, & Malyshev, 2012; Piao, Friedlingstein, Ciais, Viovy, & Demarty, 2007). Robust climate-driven models of vegetation phenology are therefore critical for projecting climate change scenarios (Cramer et al., 2001; Levis & Bonan, 2004).

Modeling springtime vegetation phenology via climate variables has received extensive attention in recent publications, and a variety of climate-driven phenological models have been proposed and tested using in-situ measurements (Cesaraccio, Spano, Snyder, & Duce, 2004; Melaas, Richardson, et al., 2013; Richardson, Bailey, Denny, Martin, & O'Keefe, 2006; Yang et al., 2012). Based on species-level observations of tree budburst, it is generally considered that temperature is the main driver for spring onsets of temperate forests (Bale et al., 2002; Chuine, Cour, & Rousseau, 1999; Hanninen & Kramer, 2007; Kaduk & Los, 2011; Wu, Gonsamo, Gough, Chen, & Xu, 2014). The temperature-based phenology models have been widely employed as sub-models in terrestrial biosphere models (Cramer et al., 2001; Kucharik et al., 2006). Most of these phenology models are empirical, with prescribed

* Corresponding author at: Tsinghua University, Mengminwei South Building Room 920, Beijing 100084, China.
E-mail address: xqcchina@gmail.com (Q. Xin).

http://dx.doi.org/10.1016/j.rse.2015.02.003
0034-4257/

values of parameters (Yang et al., 2012). However, recent studies have argued that the current model schemes do not capture the spatiotemporal variation of vegetation phenology metrics derived from satellite observations (Fisher, Richardson, & Mustard, 2007), particularly for grasslands. The responses of grasslands to local climates are more complicated than that of the forest biome. While grasses in moist environments are sensitive to temperature variation, the spring onset of dry grasslands is limited by soil water availability (Choler, Sea, Briggs, Raupach, & Leuning, 2010; De Michele, Vezzoli, Pavlopoulos, & Scholes, 2008; Liu, Tian, Hu, Hu, & Sivapalan, 2013) and often initiated by precipitation events (Ji & Peters, 2004; Lotsch, Friedl, Anderson, & Tucker, 2003; Shen, Tang, Chen, Zhu, & Zheng, 2011). Given that grassland is a key component in terrestrial biomes, it is important to further develop and refine the climate-driven phenological models for grasslands.

Though modeling grassland green-up is a research frontier in phenological studies, model development is constrained by the lack of long-term records of grass phenology from ground observations (White et al., 2009), possibly because the phenomenon of grass green-up is challenging to define with respect to tree budburst or leaf expansion (i.e., based on the percentage of leaves at their full sizes). Observations from digital cameras (Coops et al., 2012; Nijland et al., 2014) and measurements from flux towers (Melaas, Richardson, et al., 2013) provide alternative ways to infer and define the timing of vegetation green-up for specific sites, but robust model development and evaluation require sufficient site-year data. In addition to model validation using in-situ observations, there is a need for improved understanding of the spatiotemporal performance of phenology models over large geographic regions with appropriate datasets.

Satellite remote sensing provides abundant time-series observations of land surfaces for regional and global phenological studies. Vegetation indices derived from satellite observations have been shown to have close relationships with vegetation chlorophyll abundance and photosynthetic activity (Huete et al., 2002; Myneni, Hall, Sellers, & Marshak, 1995) and have proven suitable to derive key phenophases such as spring green-up and autumn browning (Fisher & Mustard, 2007; Zhang et al., 2003). Commonly used approaches that derive vegetation spring onset from satellite observations include those based on: 1) predefined thresholds of spectral vegetation indices (White, Thornton, & Running, 1997); 2) when time series of vegetation indices reach certain ratios of the seasonal amplitude (Jönsson & Eklundh, 2004), 3) the rate of increase in vegetation indices during the early growing seasons (Piao et al., 2011), and 4) higher-order derivatives of the time series of vegetation indices (Tan et al., 2011). Though the definition of spring onset varies across studies, satellite-derived spring onsets have shown good agreement with digital camera observations (Hufkens et al., 2012) and time series of CO_2 fluxes measured at tower sites (Bottcher et al., 2014).

Long-term observations from AVHRR dating back to the early 1980s have been used to quantify changes in phenology at regional and global scales (Heumann, Seaquist, Eklundh, & Jönsson, 2007; Tateishi & Ebata, 2004; White et al., 2009). However, due to sensor degradation and data quality issues, recent studies based on the AVHRR datasets have led to conflicting results concerning the trend and magnitude of phenological shifts in specific regions, such as the Tibetan Plateau (Piao et al., 2011; Wu & Liu, 2013; Zhang, Zhang, Dong, & Xiao, 2013). The coarse resolution of the AVHRR dataset also hinders validation using ground observations (Wang et al., 2011). Data from MODIS sensors with an improved signal-to-noise ratio and moderate spatial resolution have been used routinely to provide high-quality datasets (Justice et al., 2002). The product of MODIS Land Cover Dynamics (MCD12Q2) has been examined and validated in several recent studies (Ganguly, Friedl, Tan, Zhang, & Verma, 2010; Zhang et al., 2003). A relatively new time series of MCD12Q2 dataset is now available, which offers opportunities to refine and evaluate phenological models at a large scale.

The objectives of this study are to 1) use phenology metrics derived from MODIS for model refinement and validation, 2) propose a new method to characterize the spatiotemporal patterns of regional phenology variations, and 3) use flux measurements at tower sites to validate both MODIS-derived green-up dates and spring phenology models.

2. Materials and methods

2.1. Study area and data preprocessing

We performed our analysis for the Western United States (25° to 49° N, −125° to −95° W), where reliable daily climate data are available (Fig. 1). Climatic zones range from temperate in the North to tropical in the South. Temperature generally decreases with latitude and varies as a function of topography. Annual precipitation ranges widely across large areas and shows an east–west gradient. The study area includes over 95% of the grasslands in the United States and has a variety of grass species mixed with shrubs or local species of short vegetation.

To match the spatial resolution of the climate data, we preprocessed remotely sensed data from standard MODIS products and scaled up the timing of grassland green-up from MODIS resolution to a 0.125° × 0.125° resolution. Ten-year (2001–2010) data of vegetation green-up dates were extracted from the first layer of MCD12Q2 product (Ganguly et al., 2010). The timing of vegetation green-up in MCD12Q2 was derived based on the changing rates in the time series of Enhanced Vegetation Index (see for example in Fig. 2A). Because we only attempted to model springtime green-up (from Jan 1st to July 1st), areas such as California, where grass green-up begins in November and December, were not included in our analysis. The MODIS Land Cover Type product (MCD12Q1) was used to screen non-grass pixels (Friedl et al., 2002; Friedl et al., 2010). To reduce the influences of land-cover and land-use changes, we only processed pixels that were mapped as grasslands consistently in both 2001 and 2010. Apparent anomalies of grassland green-up dates within each 0.125° grid cell were excluded based on the criteria of mean ± 3 standard deviation (Roy, Jin, Lewis, & Justice, 2005). To minimize the effect of elevation on vegetation phenology, we obtained digital elevation maps from NOAA's Global Land One-km Base Elevation (GLOBE) project (Hastings & Dunbar, 1998) and excluded MODIS pixels that have an elevation exceeding mean ± 100 m of each 0.125° grid cell (Peng et al., 2014). The timing of grassland green-up for each 0.125° grid cell was then determined as the median value for all qualified MODIS observations within the corresponding grid cell. However, if the standard deviation of within-pixel grassland green-up was greater than 30 days, we excluded those grid cells for further analysis because grasses respond diversely to local climates. Because remotely sensed data contain inherent noise (Xin, Olofsson, Zhu, Tan, & Woodcock, 2013), the above processes were applied to ensure that MCD12Q2-derived grassland phenology data were of high quality for model calibration and evaluation.

Daily climate data, including photoperiod, temperature, and vapor pressure deficit, were used as forcing drivers in phenology models. To test model robustness, we processed two observational climate datasets that have been widely used in scientific research: 1) the Maurer02v2 datasets (Maurer, Wood, Adam, Lettenmaier, & Nijssen, 2002) originally developed in coordination with NASA's National Land Data Assimilation System (NLDAS) project (Maurer, personal communication; http://hydro.engr.scu.edu/files/gridded_obs/daily/ncfiles_2010/), and 2) the Daymet datasets (Thornton et al., 2012) distributed by the Oak Ridge National Laboratory (ORNL) Distributed Active Archive Center (http://daymet.ornl.gov/). To analyze the influences of soil moisture, we obtained hourly NLDAS NOAH model data achieved by NASA Goddard Earth Sciences Data and Information Services Center (ftp://hydro1.sci.gsfc.nasa.gov/). Hourly root zone (0 to 1 m for grass) soil moisture content derived from the NOAH model were averaged to daily mean values. All climate and soil moisture datasets from 2000 to 2010 were processed to daily data at a 0.125° × 0.125° resolution under the Geographic

Please cite this article as: Xin, Q., et al., Modeling grassland spring onset across the Western United States using climate variables and MODIS-derived phenology metrics, *Remote Sensing of Environment* (2015), http://dx.doi.org/10.1016/j.rse.2015.02.003

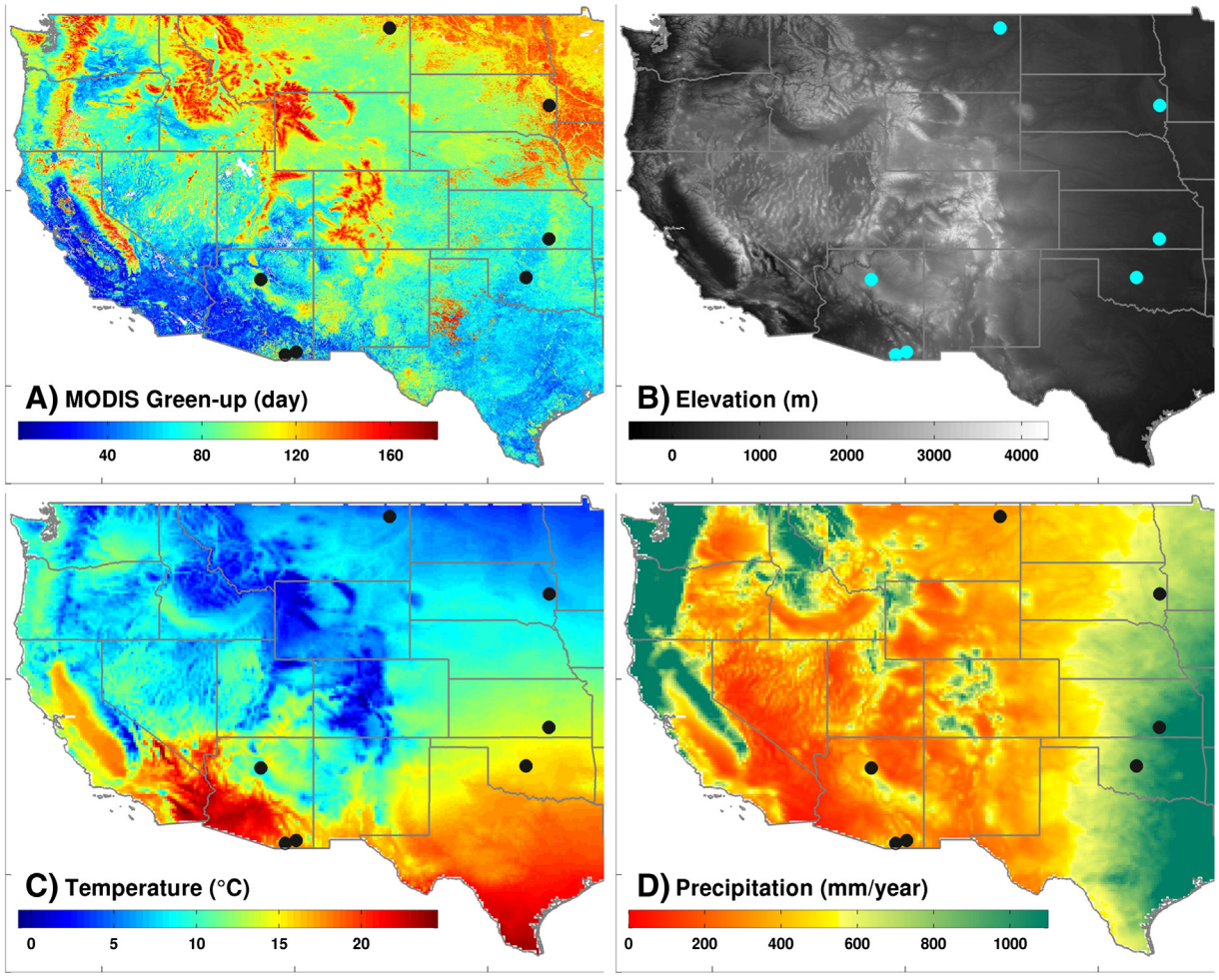

Fig. 1. Geographic distribution of (A) long-term mean springtime onset (2001–2010) derived from MODIS Land Cover Dynamics Product (MCD12Q2); (B) elevation derived from NOAA's Global Land One-km Base Elevation project; (C) long-term mean temperature (2001–2010) derived from Daymet data; and (D) long-term mean annual precipitation (2001–2010) derived from Daymet data. Solid dots denote tower sites used for ground validation (Table 1).

Lat/Lon projection. Daily mean temperature was calculated as the average of daily maximum and minimum temperatures. Daily photoperiod and vapor pressure deficit were derived following methods outlined in Allen, Pereira, Raes, and Smith (1998). Because daily vapor pressure is not available in Maurer02v2, we estimated the daily vapor pressure deficit as the difference between saturated vapor pressure at daily maximum and minimum temperatures (Lobell et al., 2014). For each year, climate data dating back to the previous September were compiled for use in spring phenology models.

Ground measurements of CO_2 flux time series at flux tower sites can be used to derive the timing of spring onsets for vegetation (Baldocchi et al., 2001). Eight grassland sites that had Level 4 data available in the

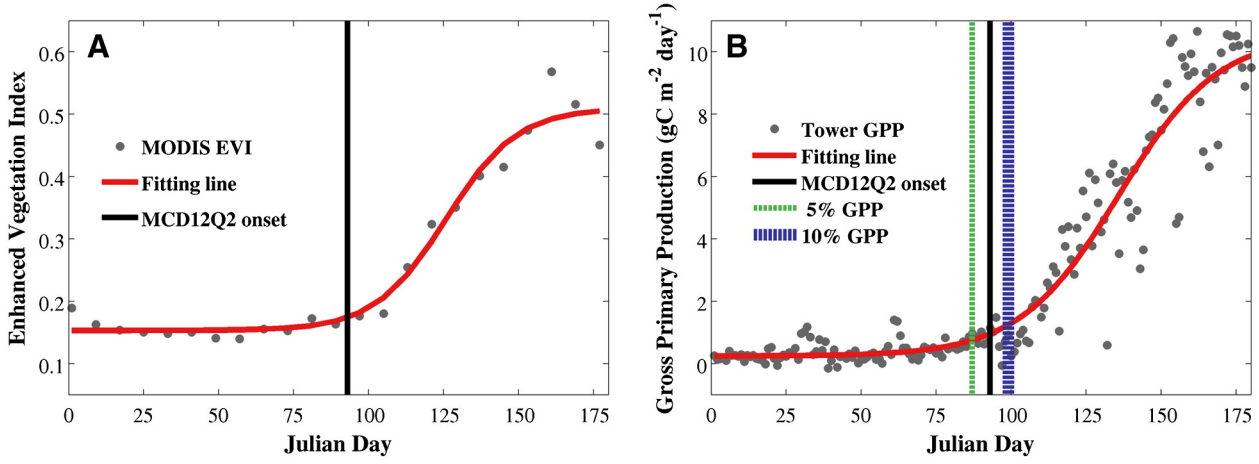

Fig. 2. Examples showing how grass green-up is derived from (A) MODIS Enhanced Vegetation Index time series and (B) flux tower CO_2 time series. Vertical lines denote the timing of derived grassland green-up. Data come from the US-Wlr site (Table 1) in 2002.

Please cite this article as: Xin, Q., et al., Modeling grassland spring onset across the Western United States using climate variables and MODIS-derived phenology metrics, *Remote Sensing of Environment* (2015), http://dx.doi.org/10.1016/j.rse.2015.02.003

AmeriFlux website (http://ameriflux.ornl.gov/) were used for ground validation (Table 1). These flux towers monitor fields of different grass types and are representative of a widespread environment in the study area. We excluded the site-year data if the Gross Primary Production (GPP) time series did not follow distinct annual cycles or the temperature data were missing for more than 10 days during springtime (Jan 1st to July 1st). Following previous studies (Zhang et al., 2003), we fit logistic lines to GPP time series and identified dates when the ratio of daily GPP to seasonal amplitude researches 5% and 10% for each site-year data (Fig. 2B). To assess the relationship between ground- and satellite-based grass green-up, we estimated the dates of MCD12Q2-derived green-up as the median value of 9 × 9 MODIS 500 m pixel windows centered on each site, excluding non-grassland pixels (Xin et al., 2012). Meteorological data measured at flux towers were processed from a half-hourly to a daily basis as forcing data for phenological models. Photoperiod for each site was calculated as a function of the latitude and the day of year, similar to our processing of regional datasets (Allen et al., 1998).

2.2. Spring phenology models

In this paper, we tested nine different models (Table 2) that predict the timing of grassland green-up based on climatic variables. The standard growing-degree day (SGDD) model, first introduced by De Réaumur (1735), is used as a phenology sub-model in several ecosystem models to predict the timing of budburst. This model simply assumes a linear relationship between the status of plant growth and energy. The grass green-up is considered to appear when heating accumulation starting from a fixed date reach a certain amount of heating-degree days. In recent modeling studies (Kucharik et al., 2006), grass green-up is predicted to occur when the accumulated heating-degree days on a −5 °C heating-base temperature after January 1 exceed 150 °C.

Melaas, Richardson, et al. (2013) proposed modified growing degree-day (MGDD) models by including a photoperiod trigger and by varying critical forcing thresholds as a function of long-term mean temperature, of which three derivative models were tested here. In the first model (MGDD1), the critical forcing threshold was varied as a linear function of long-term mean annual GDD, which accommodated to the fact that warmer areas need larger thermal summations (White et al., 1997). We used a long-term mean annual GDD instead of a long-term mean temperature to ensure a positive slope factor in the regression. In the second model (MGDD2), heating accumulation began when the daily photoperiod was greater than the photoperiod trigger (a threshold of p_0), which allowed the initiation of heating accumulation to vary along latitudes. If the minimum photoperiod was always greater than the photoperiod trigger, the heating accumulation was assumed to start from December 21, the day with the shortest photoperiod in the Northern Hemisphere. In the third model (MGDD3), we employed both photoperiod and long-term annual GDD factors to test model performance over large geographic areas.

Models that are more complex consider chilling effects on bud dormancy in addition to heating effects to predict the timing of spring onsets (Chuine, Cour, & Rousseau, 1998; Yang et al., 2012). The Sequential (SEQ) model assumes that chilling accumulation initiates when the air temperature falls below a chilling base temperature (T_{chill}) and heating accumulation starts after the chilling requirement is fulfilled. In comparison, the Parallel (PAR) model assumes that heating accumulation occurs concurrently with chilling fulfillment and spring onset occurs when heating accumulation reaches a critical sum of heating units. Both models employ T_{chill} to trigger the processes of chilling accumulation. However,

Table 2
Model descriptions.

Model code	Model name	Equations
SGDD	Standard growing-degree day	t_{SOS} such as $S_f = \sum_{t_0}^{t_{SOS}} max(x_t - T_{heat}, 0) = F^*$
MGDD1	Modified growing-degree day 1	t_{SOS} such as $S_f = \sum_{t_0}^{t_{SOS}} max(x_t - T_{heat}, 0) = a\overline{GDD} + b = F^*$
MGDD2	Modified growing-degree day 2	t_0 such as $Photo = p_0$ t_{SOS} such as $S_f = \sum_{t_0}^{t_{SOS}} max(x_t - T_{heat}, 0) = F^*$
MGDD3	Modified growing-degree day 3	t_0 such as $Photo = p_0$ t_{SOS} such as $S_f = \sum_{t_0}^{t_{SOS}} max(x_t - T_{heat}, 0) = a\overline{GDD} + b = F^*$
SEQ	Sequential	t_0 such as $S_c = \sum^{t_0} max(x_t < T_{chill}, 0) = C^*$ t_{SOS} such as $S_f = \sum_{t_0}^{t_{SOS}} max(x_t - T_{heat}, 0) = F^*$
PAR	Parallel	$S_c = \sum^{t_{SOS}} max(x_t < T_{chill}, 0) = C^*$ $W = min(S_c / C^*, 1)$ t_{SOS} such as $S_f = \sum^{t_{SOS}} [W \cdot max(x_t - T_{heat}, 0)] = F^*$
SGSI	Standard growing season index	$iTMIN = min\left(max\left(\frac{TMIN - TMIN_{Min}}{TMIN_{Max} - TMIN_{Min}}, 0\right), 1\right)$ $iVPD = min\left(max\left(1 - \frac{VPD - VPD_{Min}}{VPD_{Max} - VPD_{Min}}, 0\right), 1\right)$ $iPhoto = min\left(max\left(\frac{Photo - Photo_{Min}}{Photo_{Max} - Photo_{Min}}, 0\right), 1\right)$ $GSI = iTMIN \times iVPD \times iPhoto$ t_{SOS} such as $\overline{GSI} = G^*$
AGSI1	Accumulated growing season index 1	$GSI = iTMIN \times iVPD \times iPhoto$ t_{SOS} such as $\sum^{t_{SOS}} GSI = G^*$
AGSI2	Accumulated growing season index 2	$iSWC = min\left(max\left(\frac{SWC - SWC_{Min}}{SWC_{Max} - SWC_{Min}}, 0\right), 1\right)$ $GSI = iTMIN \times iSWC \times iPhoto$ t_{SOS} such as $\sum^{t_{SOS}} GSI = G^*$

* t_{SOS} [days] is the date of start-of-season (SOS) for grassland green-up; t_0 [days] is the starting date of heating accumulation; x_t [°C] is the air temperature at the time of day t; T_{heat} and T_{chill} [°C] are the heating- and chilling-base temperature, respectively; S_f and S_c [°C] are the accumulated heating and chilling forcing units, respectively; C^* [°C] is the critical threshold of the chilling process; $\overline{GDD}$ [°C] is long-term mean annual growing degree days with base temperature of 0 °C; a and b are regression coefficients; and F^* [°C] and G^* [dimensionless] are both critical thresholds for the heating forcing process. *TMIN* [°C] is daily minimum temperature; *VPD* [kPa] is daily vapor pressure deficit; *Photo* [hours] is daily photoperiod; *SWC* [kg/m^2] is daily mean root zone soil water content; *iTMIN, iVPD, iPhoto*, and *iSWC* [dimensionless] are the scalars for daily minimum temperature, daily vapor pressure deficit, daily photoperiod, and daily root zone soil water content, respectively, and all scalars are bounded between 0 and 1. *GSI* is the Growing Season Index and $\overline{GSI}$ is the 21-day running averages of the Growing Season Index.

Table 1
Information for the study tower sites as obtained from the AmeriFlux website.

Site code	Site name	Lat (°N)	Lon (°W)	Elev (m)	Vegetation type	No. year	Reference
US-ARb	ARM SGP Burn	35.5497	−98.0402	424	C4/C3 mixed grasses	1	Fischer, Billesbach, Berry, Riley, and Torn (2007)
US-Arc	ARM SGP Control	35.5465	−98.0401	424	C4/C3 mixed grasses	1	Fischer et al. (2007)
US-Aud	Audubon Research Ranch	31.5907	−110.5092	1469	Desert grassland	2	Xiao et al. (2010)
US-Bkg	Brookings	44.3453	−96.8362	510	Temperate grassland	2	Xiao et al. (2010)
US-FPe	Fort Peck	48.3077	−105.1019	634	Temperate grassland	5	Gilmanov et al. (2005)
US-Fwf	Flagstaff Wildfire	35.4454	−111.7718	2270	Herbaceous species	2	Dore et al. (2008)
US-Wkg	Kendall Grassland	31.7365	−109.9419	1531	C4 grasses with shrubs	1	Scott (2010)
US-Wlr	Walnut River	37.5208	−96.8550	408	C4/C3 mixed grassland	3	Coulter et al. (2006)

Please cite this article as: Xin, Q., et al., Modeling grassland spring onset across the Western United States using climate variables and MODIS-derived phenology metrics, *Remote Sensing of Environment* (2015), http://dx.doi.org/10.1016/j.rse.2015.02.003

for areas where the air temperature is always greater than the chilling base temperature, we prescribed the heating accumulation to start from December 21 (Melaas, Richardson, et al., 2013). In this case, both models are functionally equivalent to the MGDD2 model when its requirement for the photoperiod trigger (p_0) is never met.

The standard Growing Season Index (SGSI) model, originally developed by Jolly, Nemani, and Running (2005), combines a common set of climatic variables for modeling vegetation phenology. SGSI considers three key environmental variables on plant growth and canopy development, in which GSI is calculated as the product of scalars of photoperiod, minimum temperature, and vapor pressure deficit. The model parameters are prescribed empirically from previous literature and site calibrations. The moving average of SGSI has shown to be strongly correlated with satellite-derived time series of Normalized Difference Vegetation Index (Jolly et al., 2005). The spring onset was predicted to occur when the 21-day moving average of the GSI reaches 0.5.

In addition, we tested new methods that combine the concepts of the SGSI and SGDD models and accumulate GSI instead of temperature to track the suitability of the climatic environment. In the first model (AGSI1), the photoperiod mainly served as a scalar for initiating accumulation, and the temperature was normalized to account for the energy requirements of vegetation spring onset. Vapor pressure deficit, as an indicator of surface dryness (Jolly et al., 2005), was used to characterize the influence of water availability: in moist environments where water has fewer limitations on canopy development, the scalar of vapor pressure deficit is close to 1, whereas the scalar of vapor pressure deficit is close to 0 in dry areas, reflecting the limitation of water availability on vegetation growth. The spring onset was predicted to occur when the GSI accumulation reaches a critical threshold. The second model (AGSI2) was similar to AGSI1, but used root zone soil water content instead of vapor pressure deficit as an indicator of water availability. Here, we simply used a linear ramp function to represent the limitation of soil water content similar to other environmental stresses.

It is worth noting that AGSI models can be generalized and rearranged as:

$$t_{SOS} \text{ such as } \sum^{t_{SOS}} (TMIN - TMIN_{Min}) \times \prod f(x_i) = G^*(TMIN_{Max} - TMIN_{Min}) = F^* \quad (1)$$

where $f(x_i)$ [dimensionless] are scalar functions that down-regulate temperature summation; t_{SOS} [days] is the date of start-of-season (SOS) for grassland green-up; $TMIN$ [°C] is daily minimum temperature, $TMIN_{Max}$ [°C] is the capped temperature for daily minimum temperature when temperature does not limit grass growth and $TMIN_{Min}$ [°C] is the base temperature for daily minimum temperature; and $F^* = G^*(TMIN_{Max} - TMIN_{Min})$ [°C] is the critical threshold for the heating forcing process.

In essence, AGSI models are similar to SGDD models and accumulate temperatures, but they apply a multiple-constraint model of $\prod f(x_i)$ to synthesize the influences of various environmental stresses. Under unsuitable environmental conditions, effective temperature accumulation becomes smaller, such that more days are required to meet a critical threshold for initiating vegetation growth. In this way, effective GDD accumulation has an analogous form to the Jarvis–Stewart equation (Jarvis & McNaughton, 1986), which has been widely used to describe the responses of stomatal conductance to environmental factors (Ding, Kang, Du, Hao, & Zhang, 2014; Lammertsma et al., 2011; Leuning, 1995). In this study, we mainly considered the influences of water availability and photoperiod, such that $\prod f(x_i) = f(W) \times f(P)$, where $f(W)$ and $f(P)$ represent scalars that account for the limitations of water availability and photoperiod, respectively.

2.3. Model parameterization and validation

We used all pixel-years phenology metrics of grassland derived from MODIS to calibrate phenology models except two benchmark models of SGDD and SGSI. Because each model had three or more parameters, we used the Shuffled Complex Evolution Approach (Duan, Gupta, & Sorooshian, 1993; Duan, Sorooshian, & Gupta, 1992) to speed up the model calibration process without exploring the entire parameter spaces. The Root Mean Squared Error (RMSE) between modeled and MODIS-derived green-up dates served as the cost function in model optimization (Eq. (2)). Because our study area was relatively large, we used Willmott's method (Willmott et al., 1985) to correct RMSE calculations by accounting for the latitudinal variation in the grid-cell size. To optimize global parameters, we employed the Monte Carlo technique (Metropolis, Rosenbluth, Rosenbluth, Teller, & Teller, 1953) by repeating the optimization process with random initial input values. If models with varied parameter sets achieved similar performances ($\Delta RMSE < 0.5$ day), we chose the parameter set that provided the smallest biases, which were calculated as the mean difference between modeled and observed dates of spring onset (Eq. (3)).

We validated phenology models using 1) all pixel-year dates of grassland spring onset that are derived from MCD12Q2 and 2) all site-year dates of grassland spring onset that are derived from flux tower CO_2 time series. Following previous studies (Melaas, Richardson, et al., 2013), a fourfold cross-validation was performed to evaluate the out-of-sample model accuracy for each model. We performed Pearson's correlations and two-tailed Student's t-tests for model evaluation, and used the metrics of RMSE, Bias, and Mean Absolute Error (MAE) for error analysis.

$$RMSE = \sqrt{\sum w_j \left(t'_{SOS,j} - t_{SOS,j}\right)^2 / \sum w_j} \quad (2)$$

$$Bias = \sum w_j \left(t'_{SOS,j} - t_{SOS,j}\right) / \sum w_j \quad (3)$$

$$MAE = \sum w_j \left|t'_{SOS,j} - t_{SOS,j}\right| / \sum w_j \quad (4)$$

where $t'_{SOS,j}$ and $t_{SOS,j}$ are modeled and observed dates of the start-of-season (SOS) for grassland green-up, respectively; the subscript j refers to an observation in time and space; and $w_j = \cos(L)$ is a scalar weight for correcting pixel sizes given that observation j varies spatially at a latitude of L.

3. Results

3.1. Model performance using MCD12Q2-derived phenology metrics

Table 3 compares the performances of climate-driven phenological models against grassland green-up dates derived from MCD12Q2. Both Maurer02v2 and Daymet climate datasets were used for model predictions. These results indicate that two benchmark models (SGDD and SGSI) make inaccurate predictions for the timing of grassland spring onsets. The RMSE values are consistently higher than 40 days for both models. SGDD tends to have large negative biases and SGSI tends to have positive biases (approximately 4–7 weeks) for grassland onsets. After model calibrations, MGDD and AGSI models perform considerably better with RMSE values less than 20 days and low bias values. By introducing a photoperiod trigger, MGDD2 and MGDD3 perform slightly better than MGDD1. The performances of MGDD models for grassland are comparable to those for evergreen needleleaf forest or deciduous broadleaf forest presented in the work of Melaas, Richardson, et al. (2013). However, both the SEQ and PAR models result in slightly higher RMSE and MAE than the MGDD and AGSI models.

In addition to error analysis, we performed Pearson's correlations between modeled and MCD12Q2-derived dates of springtime onsets for each individual pixel, in which significant positive correlations indicate that phenology models are capable of capturing the 10-year (2001–2010) variation of the timing of grassland spring onsets. The spatial patterns shown in Fig. 3 suggest that SGDD only captures the

Please cite this article as: Xin, Q., et al., Modeling grassland spring onset across the Western United States using climate variables and MODIS-derived phenology metrics, *Remote Sensing of Environment* (2015), http://dx.doi.org/10.1016/j.rse.2015.02.003

Table 3
The performance of climate-driven models of spring phenology as evaluated against MCD12Q2-derived phenology metrics. All pixel-year spring onset dates derived from MCD12Q2 are used for model optimization and evaluation. Two climate datasets of Maurer02v2 and Daymet are used for spring onset predictions with the same parameter sets. Soil water content data from NLDAS NOAH models are used in AGSI2 model. The two values for environmental parameters listed for the SGSI and AGSI models correspond to the lower and upper limits. The two values of F^* listed for MGDD1 and MGDD3 correspond to the coefficients in $F^* = a\overline{GDD} + b$, where $\overline{GDD}$ denotes long-term mean annual GDD. Negative biases indicate that modeled spring onsets are earlier than observed ones, whereas positive biases indicate the opposite.

Model	Maurer02v02			Daymet			Optimized model parameters							
	RMSE (day)	Bias (day)	MAE (day)	RMSE (day)	Bias (day)	MAE (day)	P_0 (hour)	T_h (°C)	T_c (°C)	C^* (°C)	F^* (°C)	VPD (kha)	SWC (kg/m^2)	G^*
SGDD[a]	41.6	−35.1	35.3	45.3	−39.6	39.7		−5.0			150			
MGDD1	18.9	8.2	14.9	18.6	5.4	14.3		−5.0			0.087 196			
MGDD2	16.5	1.7	11.7	16.6	0.2	11.7	10.7	−0.8			125			
MGDD3	16.4	2.2	11.7	16.7	0.5	11.8	10.7	−0.7			0.010 91			
SEQ	19.9	5.2	15.2	18.9	1.3	13.9		−5.9	10.0	56	586			
PAR	19.9	5.8	15.3	18.5	1.5	13.7		−6.6	9.2	83	792			
SGSI[b]	67.8	33.0	56.7	44.2	36.2	38.5	10.0 11.0	−2.0 5.0				0.90 4.1		0.5
AGSI1	18.5	7.8	13.7	17.1	1.2	12.0	10.3 11.3	−7.2 1.5				1.15 3.0		12.3
AGSI2	17.9	6.3	13.1	17.5	1.9	12.4	10.3 11.3	−7.2 1.2					36.4 216	12.4

[a] Model parameter values are from Kucharik et al. (2006).
[b] Model parameter values are from Jolly et al. (2005).

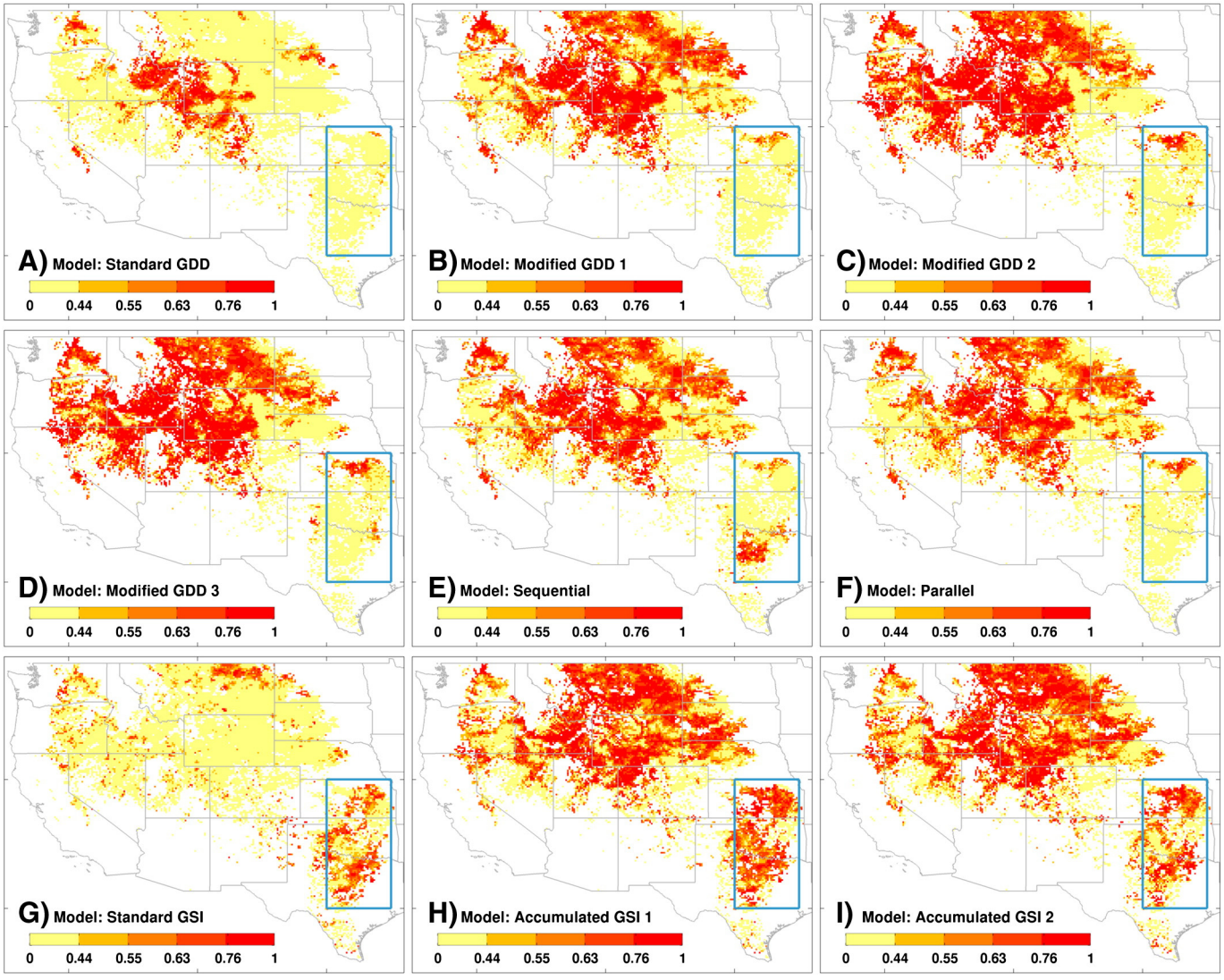

Fig. 3. Pearson's correlation coefficients between 10-year dates of spring onsets derived from MCD12Q2 and simulated by (A) Standard GDD, (B) Modified GDD 1, (C) Modified GDD 2, (D) Modified GDD 3, (E) Sequential, and (F) Parallel models, (G) Standard GSI, (H) Accumulated GSI 1, and (I) Accumulated GSI 2. The Maurer02v2 climate datasets are used for model predictions. The labels on the color bars R = 0.76, R = 0.63, R = 0.55 and R = 0.44 correspond to the 1%, 5%, 10%, and 20% significance levels, respectively. Note the difference between model performances in the subset of the cyan box (30° to 40° N, −100° to −95° W). (For interpretation of the references to color in this figure legend, the reader is referred to the web version of this article.)

Please cite this article as: Xin, Q., et al., Modeling grassland spring onset across the Western United States using climate variables and MODIS-derived phenology metrics, *Remote Sensing of Environment* (2015), http://dx.doi.org/10.1016/j.rse.2015.02.003

temperature influences on spring onsets in mountainous areas. By introducing a photoperiod trigger and accounting for the spatial variation of long-term annual GDD, MGDD models improve model performance over large geographic areas (Fig. 3B, C, and D for MGDD1, MGDD2, and MGDD3, respectively). The correlations between spring onsets predicted by MGDD models and observed by MODIS are strong in the north of the study area, but are weak in specific regions (i.e., the cyan box in Fig. 3), where generally have less annual precipitation than other areas (Fig. 1D). The SGSI model captures some temporal variations in the subset area, but does not perform well across other areas. AGSI1 and AGSI2 can model the inter-annual variation of spring onsets well across the Western US, likely due to the inclusion of vapor pressure deficit or soil moisture content. The results for both SEQ and PAR are similar in terms of the spatial pattern, but only perform reasonably well in temperature-limited areas.

Fig. 4 further compares the time series anomaly of observed and modeled spring onsets from 2001 to 2010. The mean spring onset anomalies were calculated as absolute values of timing of springtime onset minus long-term means for the entire area and for the example sub-region, respectively. The two-tailed Student's t-tests for 10-year trends (Table 4) show that only the onset anomalies modeled by AGSI2 are statistically significant for the entire areas and the sub-region. Though some models capture the general trend of the entire area, they may not be used for predicting inter-annual phenology variation over specific regions, where water availability plays a vital role in the timing of grassland onsets. The results presented here imply that explicit inclusion of water availability in phenology models could potentially improve their performances for grasslands.

To test the robustness of phenology models, we also performed the same analysis using Daymet climate datasets. The results in terms of error analysis (Tables 3 and 4), the spatial pattern of the correlation coefficient (Fig. 5), and general trends (Fig. 6) are very similar to those obtained using the Maurer02v2 climate dataset. These results illustrate that high-quality climate datasets and satellite observations could provide a robust basis for phenology model calibration and refinement at large scales.

3.2. Ground validation using eddy covariance data

Fig. 7 shows good agreement between green-up dates derived from MODIS observations and flux tower measurements, though their green-up dates are defined somewhat differently. The satellite-derived green-

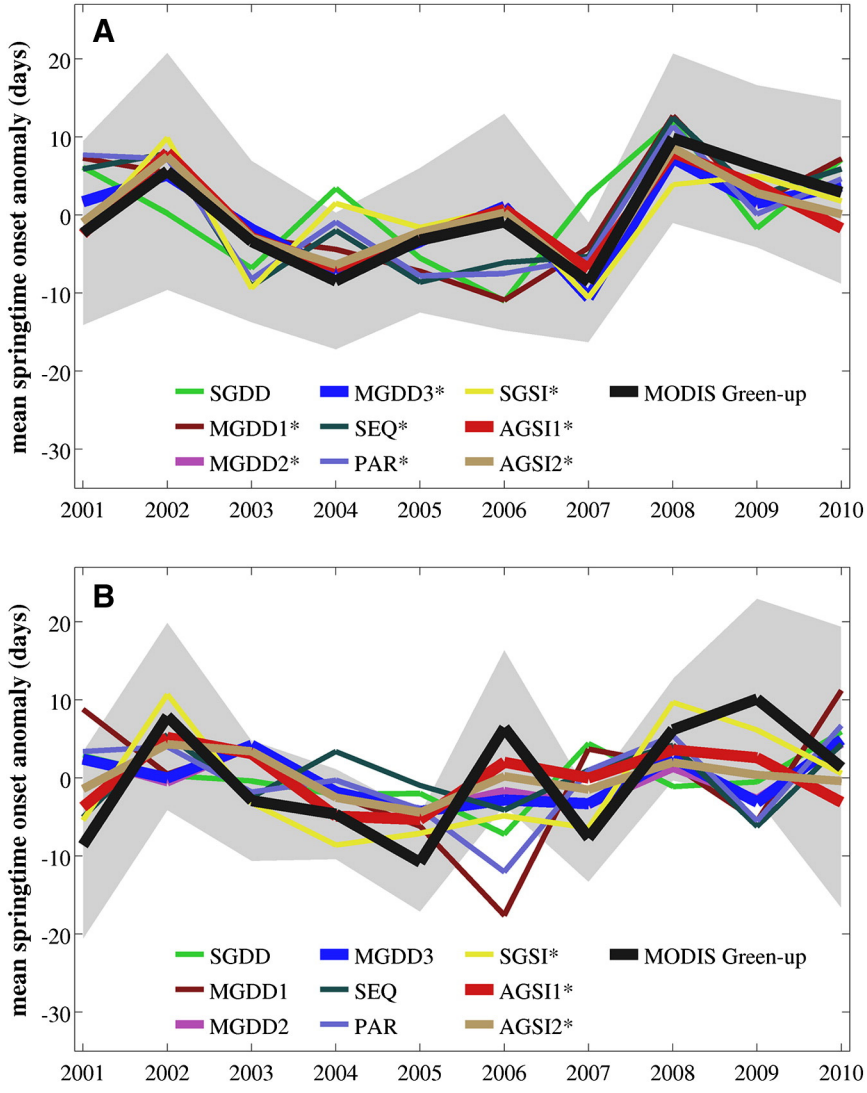

Fig. 4. The ten-year (2001–2010) anomaly of grassland spring onsets as derived from MCD12Q2 and different models shown for (A) the entire area and (B) the subset of the cyan box (30° to 40° N, −100° to −95° W) in Fig. 3. The Maurer02v2 climate datasets are used for model predictions. Root zone (0 to 1 m) soil water content data from the NLDAS NOAH model are used in the AGSI2 model. Shaded areas denote ± standard deviation for MODIS observations. Pearson's correlations and two-tailed Student's t-tests are performed between observed and modeled springtime onsets. The asterisks indicate that the correlation between modeled and MODIS-derived timing of spring onset is significant at the 0.05 level.

Please cite this article as: Xin, Q., et al., Modeling grassland spring onset across the Western United States using climate variables and MODIS-derived phenology metrics, *Remote Sensing of Environment* (2015), http://dx.doi.org/10.1016/j.rse.2015.02.003

Table 4
Pearson's correlation coefficient (r) for the ten-year (2001–2010) anomaly of grassland spring onsets as derived from MCD12Q2 and different models. This table summarizes all results in Figs. 4 and 6. The sub-region area (30° to 40° N, −100° to −95° W) is shown as the cyan box in Fig. 3. Probabilities for two-tailed Student's t-tests are given in parenthesis.

Model	Entire area		Sub-region	
	Maurer02v2	Daymet	Maurer02v2	Daymet
SGDD	0.295 ($p = 0.408$)	0.197 ($p = 0.586$)	−0.288 ($p = 0.419$)	−0.318 ($p = 0.370$)
MGDD1	0.677 ($p = 0.032$)[a]	0.654 ($p = 0.040$)[a]	−0.312 ($p = 0.380$)	−0.346 ($p = 0.327$)
MGDD2	0.915 ($p < 0.001$)[c]	0.894 ($p < 0.001$)[c]	0.081 ($p = 0.823$)	0.072 ($p = 0.843$)
MGDD3	0.914 ($p < 0.001$)[c]	0.893 ($p < 0.001$)[c]	0.085 ($p = 0.816$)	0.077 ($p = 0.832$)
SEQ	0.738 ($p = 0.015$)[a]	0.697 ($p = 0.025$)[a]	0.079 ($p = 0.827$)	0.089 ($p = 0.806$)
PAR	0.648 ($p = 0.043$)[a]	0.595 ($p = 0.070$)	−0.119 ($p = 0.744$)	−0.157 ($p = 0.665$)
SGSI	0.713 ($p = 0.021$)[a]	0.765 ($p = 0.010$)[a]	0.798 ($p = 0.006$)[b]	0.553 ($p = 0.097$)
AGSI1	0.935 ($p < 0.001$)[c]	0.939 ($p < 0.001$)[c]	0.753 ($p = 0.012$)[a]	0.617 ($p = 0.057$)
AGSI2	0.953 ($p < 0.001$)[c]	0.930 ($p < 0.001$)[c]	0.675 ($p = 0.032$)[a]	0.643 ($p = 0.045$)[a]

[a] Correlation is significant at the 0.05 level.
[b] Correlation is significant at the 0.01 level.
[c] Correlation is significant at the 0.001 level.

up dates are significantly correlated with dates defined based on a 5% GPP ratio ($r = 0.665$; $p = 0.0036$) or a 10% GPP ratio ($r = 0.761$; $p = 0.0004$). Green-up from MCD12Q2 has lower biases (−2.2 versus 5.6 days) and smaller RMSE (14.7 versus 18.3 days) relative to the timing of the 10% GPP ratio than the timing of the 5% GPP ratio. These results demonstrate the usefulness of satellite observations for scaling-up the timing of grassland spring onset.

Using climate data measured at the flux towers, the climate-driven models of spring phenology are able to make reasonable predictions for grassland spring onsets (Fig. 8). Because we calibrate phenology models with MODIS data, it is not surprising that the modeled results match the satellite observations better than flux tower measurements. Overall, the timing of spring onsets modeled by AGSI could explain approximately 61.0% of the variance ($p = 0.0002$) for green-up dates

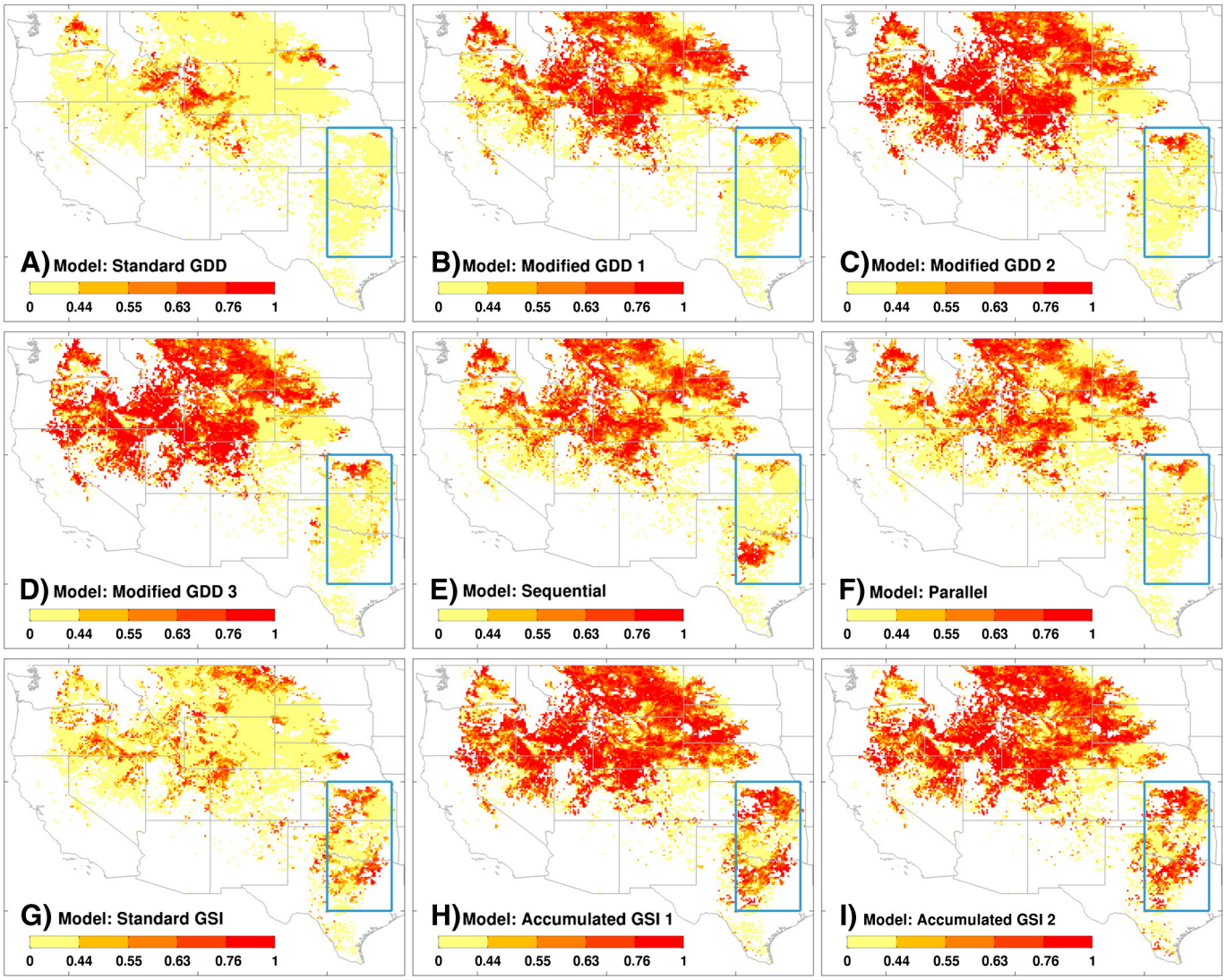

Fig. 5. Same as Fig. 3, but the Daymet climate datasets are used for model predictions.

Please cite this article as: Xin, Q., et al., Modeling grassland spring onset across the Western United States using climate variables and MODIS-derived phenology metrics, *Remote Sensing of Environment* (2015), http://dx.doi.org/10.1016/j.rse.2015.02.003

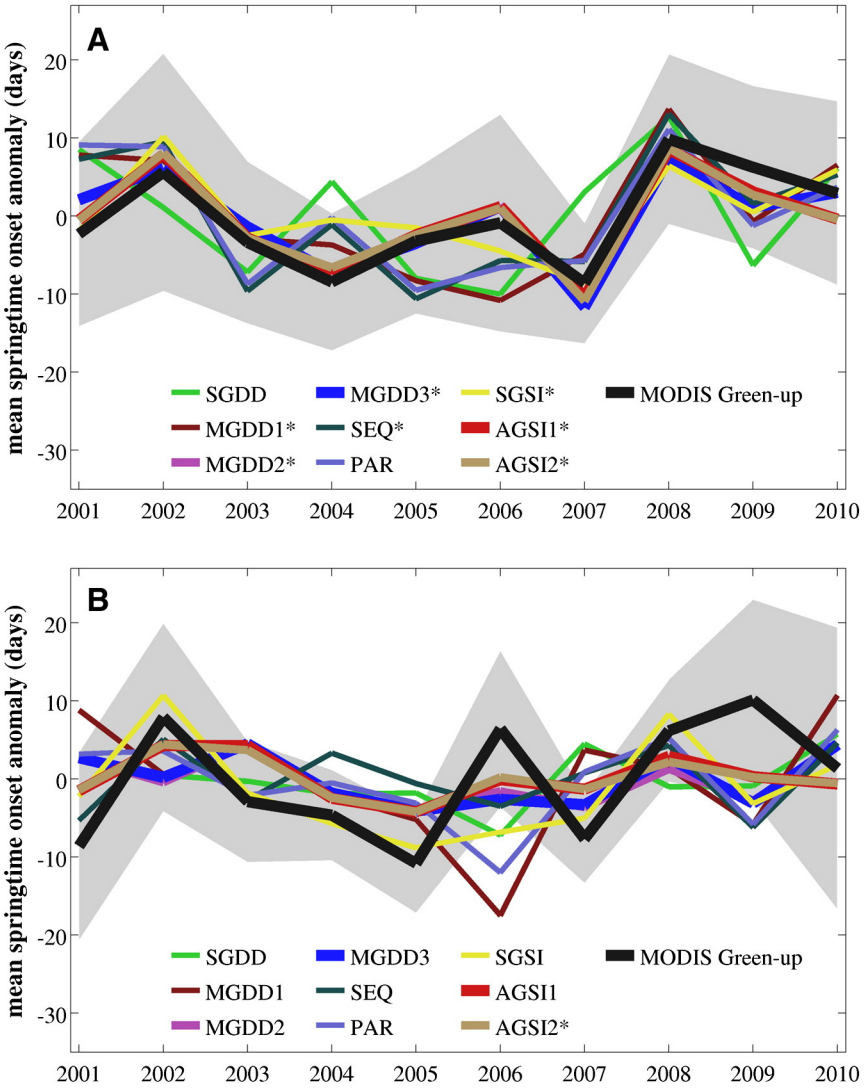

Fig. 6. Same as Fig. 4, but the Daymet climate datasets are used for model predictions.

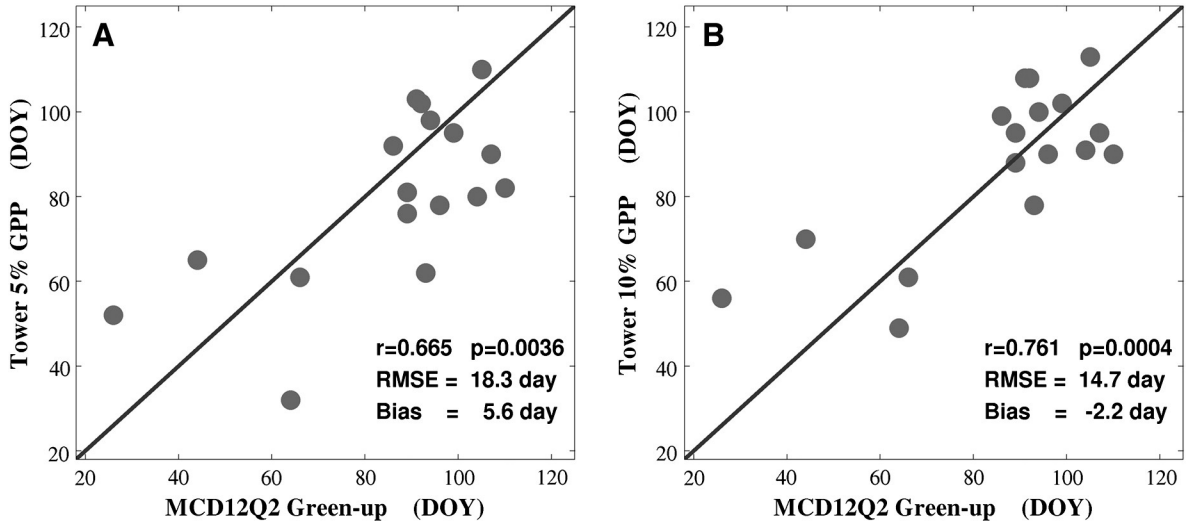

Fig. 7. Spring onset dates derived from MODIS Land Cover Dynamics Product (MCD12Q2) are validated against dates derived from flux tower data based on the criteria of (A) 5% GPP ratio and (B) 10% GPP ratio. Solid lines denote the 1:1 lines.

Please cite this article as: Xin, Q., et al., Modeling grassland spring onset across the Western United States using climate variables and MODIS-derived phenology metrics, *Remote Sensing of Environment* (2015), http://dx.doi.org/10.1016/j.rse.2015.02.003

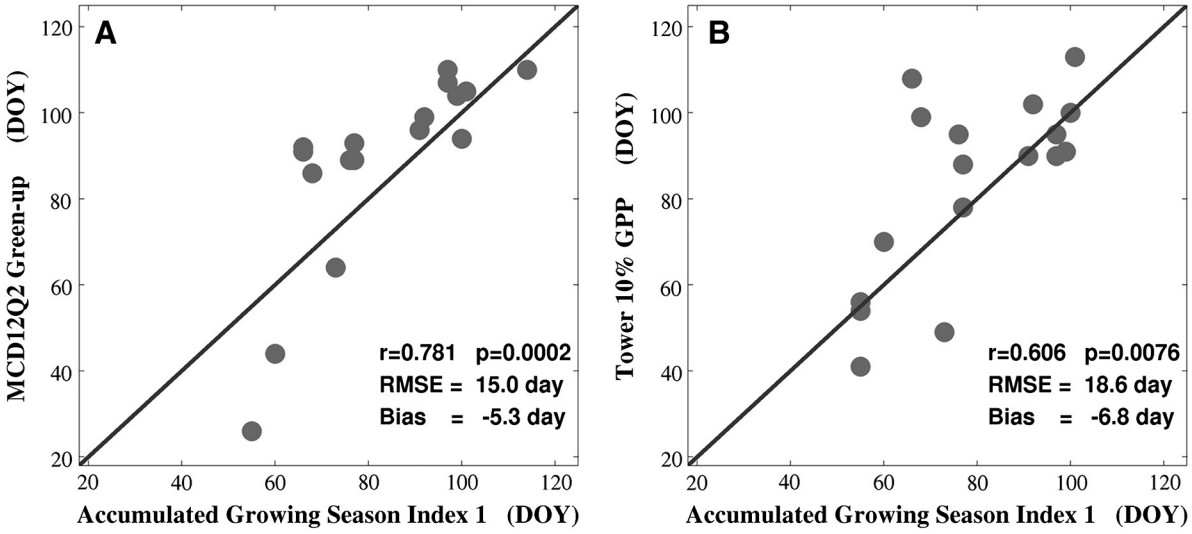

Fig. 8. Spring onset dates modeled by AGSI1 are compared with dates derived from (A) MODIS Land Cover Dynamics Product (MCD12Q2) and (B) flux tower 10% GPP ratio. Solid lines denote the 1:1 lines.

derived from MCD12Q2 and 36.7% of the variance ($p = 0.0076$) for those derived from flux towers. Table 5 summarizes the statistics for phenology models as evaluated using all site-year flux tower data. The performances for summarized models are similar at both small- and large-scales (Tables 3 and 5), supporting the robustness of our methods. However, due to limited flux towers in the study area, comprehensive ground validation requires more site-year data from tower sites when they become available.

3.3. Environmental factors in springtime phenology models

In addition to model calibration and validation, we further investigate the reasons behind the model performances. Fig. 9 plots residuals between modeled and observed springtime onsets against long-term mean annual GDD. For the SGDD model, the relationship is negatively statistically significant ($p < 0.0001$; Fig. 9A). This result implies that energy requirements for triggering grass growth could vary with geographic regions, where colder regions require less energy than warmer regions to initiate springtime green-up. The MGDD1 model, by varying the critical threshold, compensates for this effect and the probability for the correlation becomes insignificant at the 0.05 level. The MGDD2 model, by including a photoperiod trigger alone, also reduces the dependence of modeled residuals on long-term mean annual GDD, though the negative relationship is still significant at the 0.01 level. The MGDD3 model, which combines the concepts of MGDD1 and MGDD2, achieves the best performance and modeled and observed springtime onsets are insignificantly correlated ($p = 0.9653$). These results indicate that introducing varied critical thresholds and a photoperiod trigger in temperature-based phenology models could improve overall model applicability across large geographic regions.

To investigate the effects of water availability on grassland green-up, we plot residuals between modeled and observed springtime onsets against mean soil water content 30 days before MODIS-derived spring onset dates in Fig. 10. The MGDD3 model, though it performs well in most areas, shows a significant correlation ($r = 0.082$; $p < 0.0001$) between modeled residuals and 30-day leading mean soil water content. The relationship is positive, implying that drier areas require more days to initiate grass green-up. The negative relationship given by the SGSI model indicates that model calibration is necessary for current spring phenology models. Both AGSI1 and AGSI2 could remove the dependence of modeled residuals on 30-day leading mean soil water content (correlations are insignificant at the 0.01 level). These results indicate that explicit considerations of water availability are required in temperature-based phenology models to predict grassland green-up.

4. Discussion

In this study, we demonstrate the feasibility of using satellite remote sensing data for the development and refinement of grassland phenology models across the Western United States. Models calibrated against MCD12Q2 are able to make predictions for grassland spring onset

Table 5
Evaluation of spring onset models using flux tower data. The results for the Sequential and Parallel models are not presented because both models require climate data in previous years such that available site-year observations are largely reduced. The results for the AGSI2 model are not presented because soil moisture data were missing from the measurements in some sites.

Model	MCD12Q2 Green-up				Tower 5% GPP				Tower 10% GPP			
	Pearson's corr. (r)	RMSE (day)	Bias (day)	MAE (day)	Pearson's corr. (r)	RMSE (day)	Bias (day)	MAE (day)	Pearson's corr. (r)	RMSE (day)	Bias (day)	MAE (day)
SGDD	0.618[b]	39.0	−31.1	31.1	0.426	38.0	−23.8	29.6	0.446	42.9	−32.1	32.9
MGDD1	0.741[c]	16.2	2.2	13.5	0.472[a]	24.8	8.2	19.7	0.521[a]	21.5	−0.1	16.5
MGDD2	0.736[c]	17.7	1.5	14.2	0.499[a]	23.4	5.3	18.8	0.559[a]	20.8	−2.9	16.4
MGDD3	0.770[c]	15.1	−5.0	12.4	0.517[a]	20.6	1.6	15.2	0.570[a]	19.5	−6.7	13.9
SGSI	0.649[b]	32.9	22.6	27.2	0.315	42.3	25.3	32.9	0.387	36.1	17.1	27.2
AGSI1	0.781[c]	15.0	−5.3	12.8	0.563[a]	19.4	1.4	14.7	0.606[b]	18.6	−6.8	13.1

[a] Correlation is significant at the 0.05 level.
[b] Correlation is significant at the 0.01 level.
[c] Correlation is significant at the 0.001 level.

Please cite this article as: Xin, Q., et al., Modeling grassland spring onset across the Western United States using climate variables and MODIS-derived phenology metrics, *Remote Sensing of Environment* (2015), http://dx.doi.org/10.1016/j.rse.2015.02.003

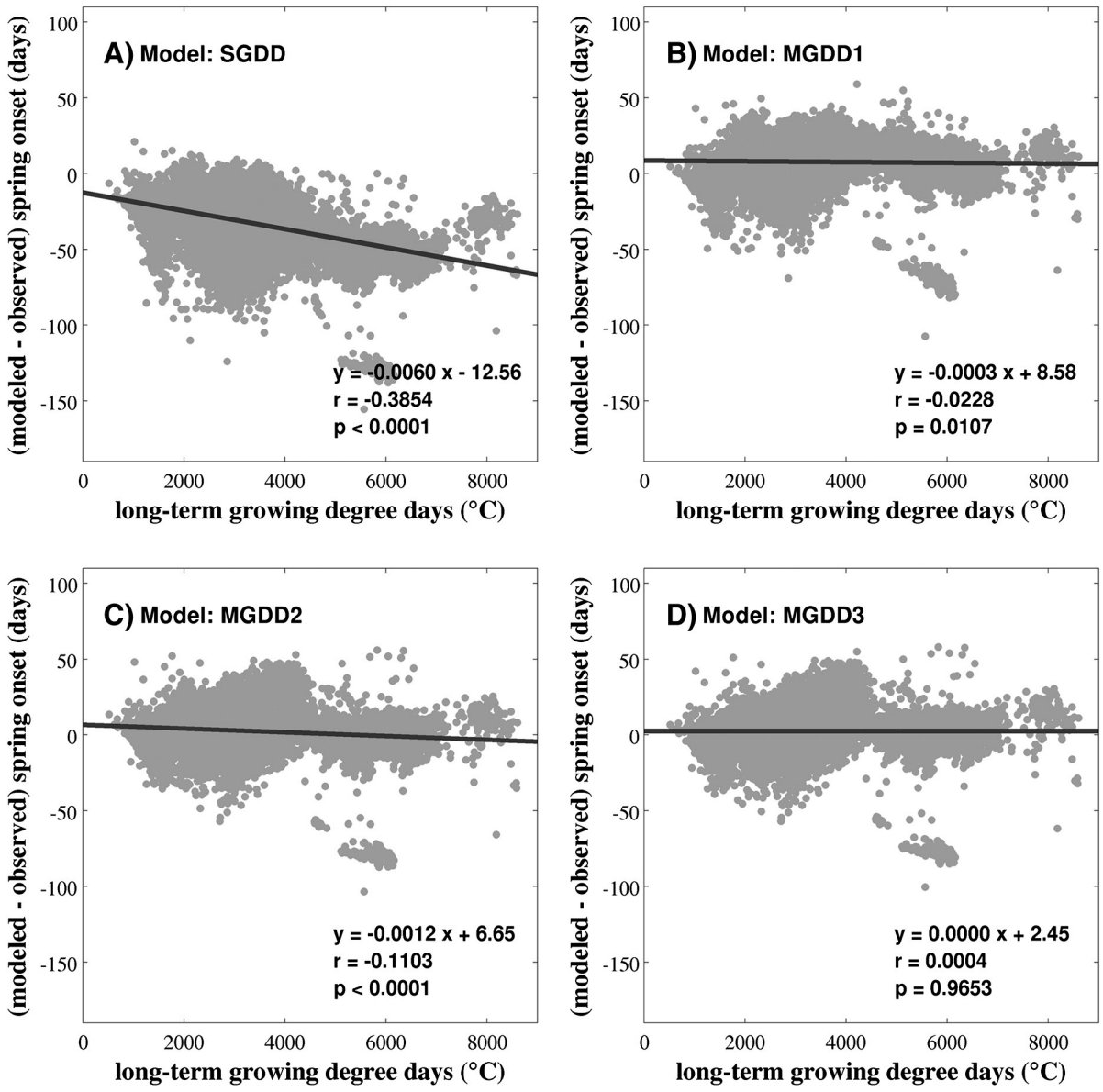

Fig. 9. Correlations between long-term mean annual growing degree-days and the residuals between modeled and observed timing of spring onsets are shown for A) SGDD, B) MGDD1, C) MGDD2, and D) MGDD3 models. Data are shown for all observations in 2010 across the entire area. Solid lines denote the regression lines.

with RMSE values less than 20 days. The achieved accuracy is reasonable considering that grasslands exhibit extensive inter-annual and within-pixel variation in vegetation dynamics in response to climate variability. Fig. 11 presents histograms for spring onset anomalies of grasslands. The frequency of pixel numbers is normally distributed. The standard deviations for spring onset anomalies are 12.4 days for inter-annual variation and 10.9 days for within-pixel variation, indicating the highly varied phenology of grasslands as derived from satellite observations. Our findings are also in line with previous studies (Kucharik et al., 2006; White et al., 1997), which suggested that a 10-day error in satellite-derived timing of vegetation green-up was reasonable.

It would be of interest to test other available models in addition to nine phenology models tested here. We have tested other variant GDD models proposed in Melaas, Richardson, et al. (2013). The parameters that vary the base temperature as a function of long-term mean temperature tend to have values very close to zero during our optimization processes (results are not shown), and we observe no apparent evidence that including these parameters would improve model performances significantly in comparison to tested MGDD models. There are also other more complex models available. Baldocchi et al. (2005) modified the phenology sub-model in the TSOIL model and used air and soil temperature to predict spring onsets of deciduous broadleaf forests. White et al. (1997) proposed empirical functions of soil temperature, air temperature, and precipitation for modeling forest and grass spring onsets. Physiologically, soil temperature and moisture have been found to influence the timing of grassland spring onsets (Jin, Zhuang, He, Luo, & Shi, 2013; Liu et al., 2013; Shen et al., 2011); therefore, including soil temperature is likely to boost model performance. Because current large-scale datasets of soil temperature and moisture such as NLDAS are derived from land-surface models such as Mosaic, Noah, VIC, and SAC (Koster & Suarez, 1992; Liang, Lettenmaier, & Wood, 1996; Luo et al., 2003; Schaake et al., 2004; Xia et al., 2012), care should be taken when calibrating phenology models with these datasets.

Due to the limited availability of the MCD12Q2 products, we only performed trend analysis for the period of 2001 to 2010. The 10-year

Please cite this article as: Xin, Q., et al., Modeling grassland spring onset across the Western United States using climate variables and MODIS-derived phenology metrics, *Remote Sensing of Environment* (2015), http://dx.doi.org/10.1016/j.rse.2015.02.003

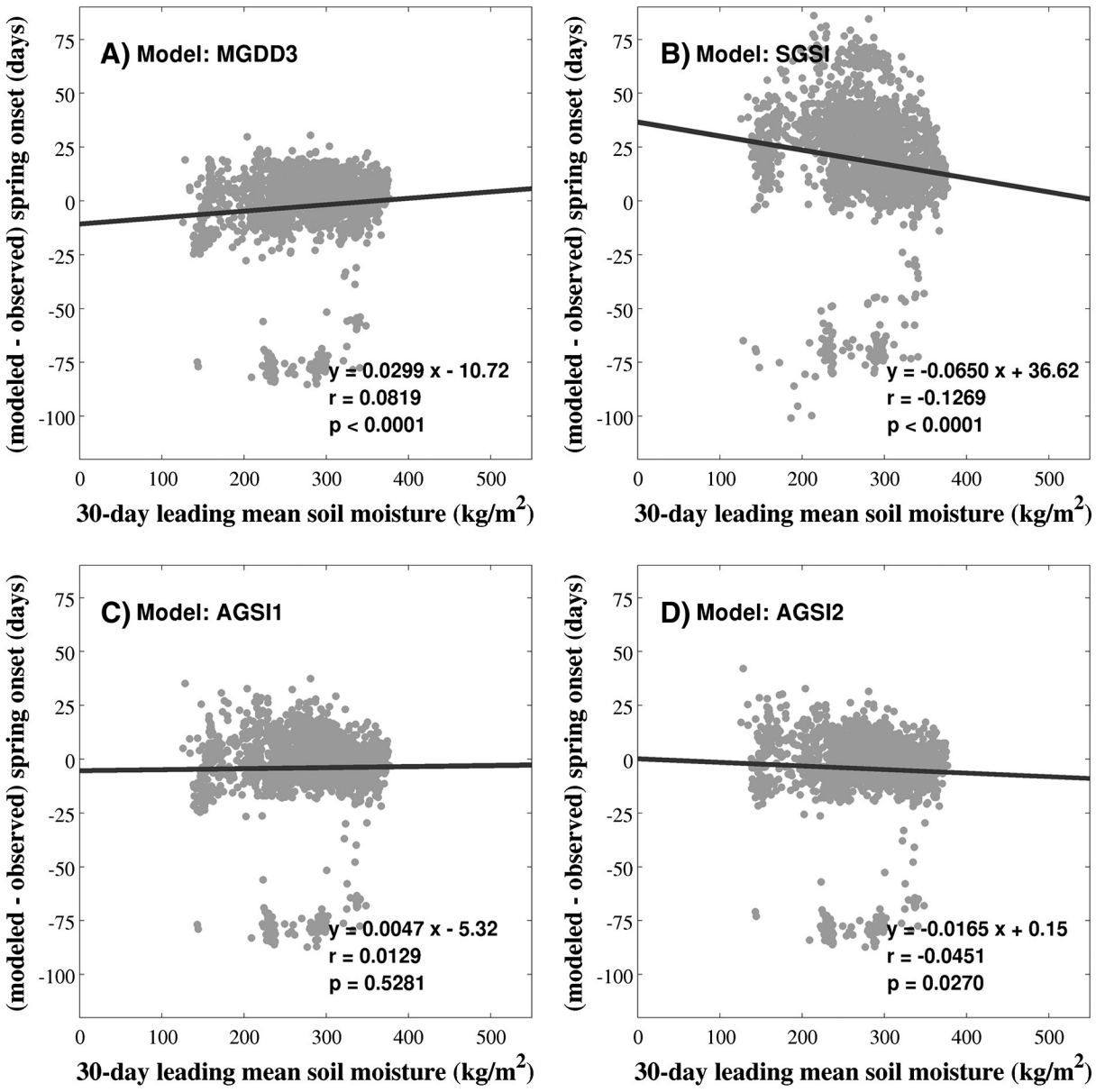

Fig. 10. Correlations between 30-day leading mean root zone (0 to 1 m) soil water content and the residuals between modeled and observed timing of spring onsets are shown for A) MGDD3, B) SGSI, C) AGSI1, and D) AGSI2 models. Data are shown for observations in 2010 over a sub-region (30° to 40° N, −100° to −95° W; the cyan box in Fig. 3). Solid lines denote the regression lines.

satellite data may not be sufficient for evaluating the predictive power of models on the inter-annual variation of grass phenology. Further analysis on the temporal ability of models requires phenology datasets constructed from longer time series of satellite data, such as Landsat or AVHRR (Zhu et al., 2013). However, recent studies have found that the data quality issues of AVHRR could influence the derived spring onsets of vegetation. On the other hand, deriving phenology metrics from higher spatial but lower temporal resolution images, such as Landsat, is challenging, though efforts have been made for small regions (Melaas, Friedl, & Zhu, 2013). Continued monitoring of land surfaces from MODIS and new satellite sensors will provide necessary datasets for further investigation.

Grasslands are often composed of a variety of grass species and are often mixed with other short vegetation. Vegetation primary productivities under different photosynthetic pathways (i.e., C3 versus C4) have varied sensitivities to ambient temperatures (Kalfas, Xiao, Vanegas, Verma, & Suyker, 2011; Xin, Broich, Suyker, Yu, & Gong, 2015). As a result, grass growth may respond diversely to climate change and variability, and regrowth is likely to occur in areas where climate permits. Multiple cycles of vegetation dynamics in a year are also apparent in our analysis of the flux tower data. However, the spring phenology models we tested here only simulate the earliest timing of grass spring onsets. This may also contribute to errors in our site validation of phenology models because vegetation types in terms of photosynthetic pathways and species composition are shown to vary across tower sites (Table 1). Predicting the onset of other cycles or cycles that do not follow an annual curve is beyond the scope of the current research and poses a challenge for future research.

5. Conclusions

Modeling grassland phenology is critical for understanding the impacts of climate variation on vegetation dynamics. However, model development requires objective datasets and sufficient samples for

Please cite this article as: Xin, Q., et al., Modeling grassland spring onset across the Western United States using climate variables and MODIS-derived phenology metrics, *Remote Sensing of Environment* (2015), http://dx.doi.org/10.1016/j.rse.2015.02.003

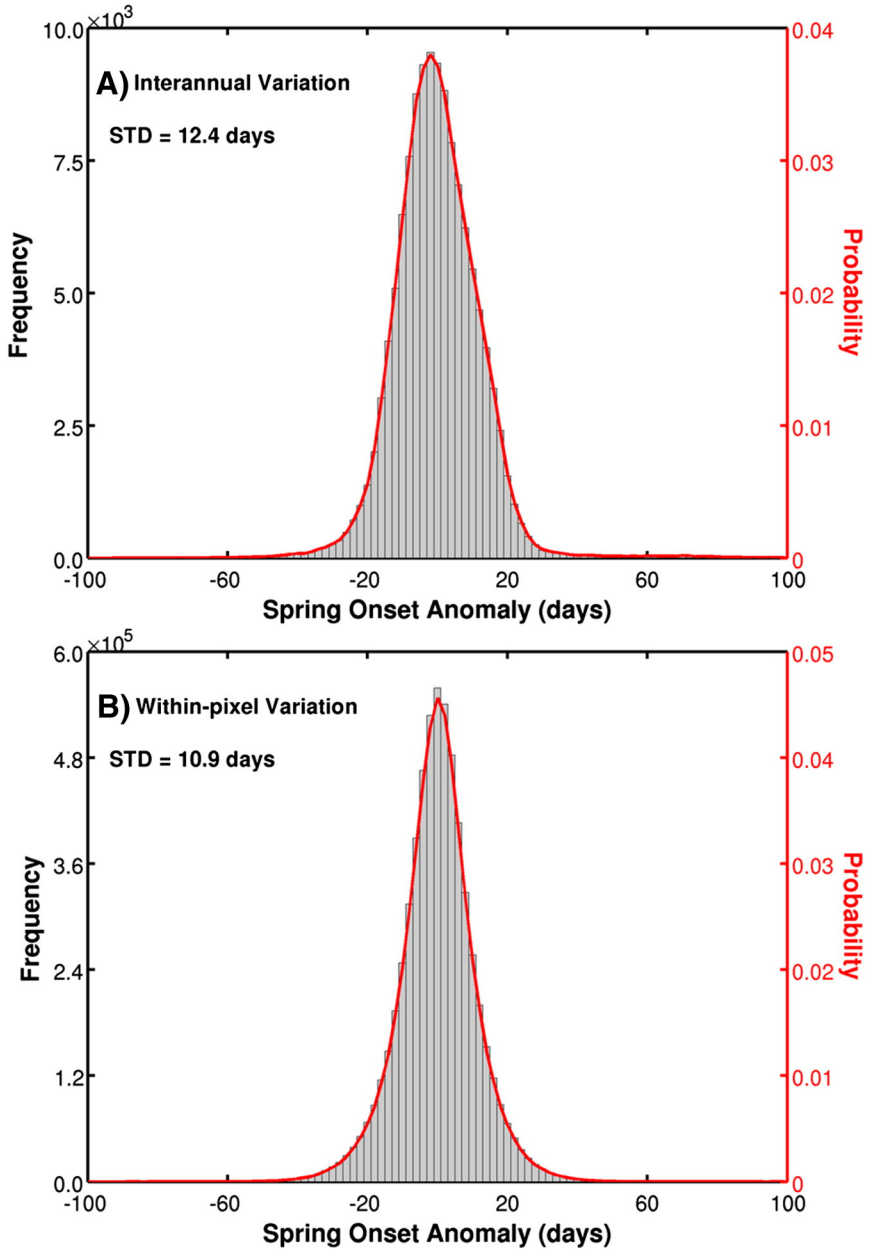

Fig. 11. The distributions of frequency and derived probability for MCD12Q2-derived grassland green-up shown for A) inter-annual and B) within-pixel variation. All observations at 0.125° resolution from 2001 to 2010 are used to derive the frequency distribution for inter-annual variation (defined as the absolute value of spring onset dates minus the long-term mean of the corresponding pixel). All observations at 500 m resolution are used to derive the frequency distribution for within-pixel variation (defined as the absolute values of spring onset dates at 500 m resolution minus the median value of the corresponding pixel at 0.125° resolution). Observation frequencies are fitted with the normal probability density function. STD denotes standard deviation.

grassland. In this study, we tested 9 phenology models and evaluated their spatiotemporal performance using phenology metrics derived from satellite observations. We carefully processed the grassland green-up dates derived from MODIS and the climate datasets. The spring phenology models were calibrated and evaluated against 10-year MODIS observations and 17 site-years flux tower measurements.

Three main conclusions are drawn from our study. First, our results confirm recent studies (Richardson et al., 2012) and indicate that the current phenology sub-model implemented in several ecosystem models is likely to misrepresent the timing of vegetation spring onsets. The standard growing-degree day (SGDD) model uses temperature accumulations and the standard Growing Season Index (SGSI) model combines a common set of climatological variables to predict the timing of grassland springtime onsets. As evaluated against MODIS observations, both the SGDD and SGSI models produce large biased errors and do not capture the inter-annual variation of vegetation dynamics over large areas. Second, careful calibration of simple variants of generalized phenology models may produce acceptable accuracies for regional models. The modified growing-degree day (MGDD) models that add a photoperiod trigger and varied critical forcing thresholds to SGDD models could improve the predictions of the spring onset of grasslands. However, MGDD models do not capture the phenology variation well over water-limited areas, suggesting that including parameters relative to water availability is necessary in phenology models. Last, we propose new methods for modeling grassland spring onset based on the accumulation of Growing Season Index. The AGSI models consider the influences of day length (photoperiod), minimum temperature (energy), and vapor pressure deficit or soil moisture (dryness) on grass growth. The results indicate that the AGSI models are able to make reasonable predictions of grass spring onsets derived from MODIS observations

Please cite this article as: Xin, Q., et al., Modeling grassland spring onset across the Western United States using climate variables and MODIS-derived phenology metrics, *Remote Sensing of Environment* (2015), http://dx.doi.org/10.1016/j.rse.2015.02.003

and flux tower measurements. Further investigation is required to understand whether the developed models can be applied to longer time series or other places in the world.

In this study, we combine satellite data and large-scale climate datasets for modeling grassland spring onsets. The use of time series MODIS data provides objective definitions of spring onsets and abundant observations that allow model development and calibration over large areas. Another advantage of this method is that model performances can be evaluated both spatially and temporally. Further research should address the issue of data quality in remotely sensed data and conduct uncertainty analysis for satellite-derived phenology metrics.

Acknowledgments

We would like to thank Dr. Eli K. Melaas at Boston University for his constructive comments. We acknowledge support from the National Natural Science Foundation of China (Grant Nos. 41401484 and 2013M540087). We gratefully thank anonymous reviewers for their insightful advice.

References

Allen, R.G., Pereira, L.S., Raes, D., & Smith, M. (1998). *Crop evapotranspiration—Guidelines for computing crop water requirements-FAO Irrigation and drainage paper 56. 300.* (pp. 6541). Rome: FAO, 6541.

Baldocchi, D.D., Black, T., Curtis, P., Falge, E., Fuentes, J., Granier, A., Gu, L., Knohl, A., Pilegaard, K., & Schmid, H. (2005). Predicting the onset of net carbon uptake by deciduous forests with soil temperature and climate data: A synthesis of FLUXNET data. *International Journal of Biometeorology*, *49*, 377–387.

Baldocchi, D., Falge, E., Gu, L., Olson, R., Hollinger, D., Running, S., Anthoni, P., Bernhofer, C., Davis, K., & Evans, R. (2001). FLUXNET: A new tool to study the temporal and spatial variability of ecosystem-scale carbon dioxide, water vapor, and energy flux densities. *Bulletin of the American Meteorological Society*, *82*, 2415–2434.

Bale, J.S., Masters, G.J., Hodkinson, I.D., Awmack, C., Bezemer, T.M., Brown, V.K., Butterfield, J., Buse, A., Coulson, J.C., & Farrar, J. (2002). Herbivory in global climate change research: Direct effects of rising temperature on insect herbivores. *Global Change Biology*, *8*, 1–16.

Bottcher, K., Aurela, M., Kervinen, M., Markkanen, T., Mattila, O.P., Kolari, P., Metsamaki, S., Aalto, T., Arslan, A.N., & Pulliainen, J. (2014). MODIS time-series-derived indicators for the beginning of the growing season in boreal coniferous forest—A comparison with CO_2 flux measurements and phenological observations in Finland. *Remote Sensing of Environment*, *140*, 625–638.

Broich, M., Huete, A., Tulbure, M.G., Ma, X., Xin, Q., Paget, M., Restrepo-Coupe, N., Davies, K., Devadas, R., & Held, A. (2014). Land surface phenological response to decadal climate variability across Australia using satellite remote sensing. *Biogeosciences*, *11*, 5181–5198.

Cesaraccio, C., Spano, D., Snyder, R.L., & Duce, P. (2004). Chilling and forcing model to predict bud-burst of crop and forest species. *Agricultural and Forest Meteorology*, *126*, 1–13.

Choler, P., Sea, W., Briggs, P., Raupach, M., & Leuning, R. (2010). A simple ecohydrological model captures essentials of seasonal leaf dynamics in semi-arid tropical grasslands. *Biogeosciences*, *7*, 907–920.

Chuine, I., Cour, P., & Rousseau, D.D. (1998). Fitting models predicting dates of flowering of temperate-zone trees using simulated annealing. *Plant, Cell and Environment*, *21*, 455–466.

Chuine, I., Cour, P., & Rousseau, D.D. (1999). Selecting models to predict the timing of flowering of temperate trees: Implications for tree phenology modelling. *Plant, Cell and Environment*, *22*, 1–13.

Churkina, G., Schimel, D., Braswell, B.H., & Xiao, X.M. (2005). Spatial analysis of growing season length control over net ecosystem exchange. *Global Change Biology*, *11*, 1777–1787.

Cleland, E.E., Chuine, I., Menzel, A., Mooney, H.A., & Schwartz, M.D. (2007). Shifting plant phenology in response to global change. *Trends in Ecology & Evolution*, *22*, 357–365.

Coops, N.C., Hilker, T., Bater, C.W., Wulder, M.A., Nielsen, S.E., McDermid, G., & Stenhouse, G. (2012). Linking ground-based to satellite-derived phenological metrics in support of habitat assessment. *Remote Sensing Letters*, *3*, 191–200.

Coulter, R.L., Pekour, M.S., Cook, D.R., Klazura, G.E., Martin, T.J., & Lucas, J.D. (2006). Surface energy and carbon dioxide fluxes above different vegetation types within ABLE. *Agricultural and Forest Meteorology*, *136*, 147–158.

Cramer, W., Bondeau, A., Woodward, F.I., Prentice, I.C., Betts, R.A., Brovkin, V., Cox, P.M., Fisher, V., Foley, J.A., & Friend, A.D. (2001). Global response of terrestrial ecosystem structure and function to CO_2 and climate change: Results from six dynamic global vegetation models. *Global Change Biology*, *7*, 357–373.

De Michele, C., Vezzoli, R., Pavlopoulos, H., & Scholes, R.J. (2008). A minimal model of soil water–vegetation interactions forced by stochastic rainfall in water-limited ecosystems. *Ecological Modelling*, *212*, 397–407.

De Réaumur, R.A.F. (1735). Observations du thermometer, faites à Paris pendant l'année 1735, comparées avec celles qui ont été faites sous la ligne, à l'Isle de France, à Alger et en quelques-unes de nos isles de l'Amérique. *Mémoires de l'Académie des Sciences*, 545–584.

Ding, R., Kang, S., Du, T., Hao, X., & Zhang, Y. (2014). Scaling up stomatal conductance from leaf to canopy using a dual-leaf model for estimating crop evapotranspiration. *PLoS ONE*, *9*, e95584.

Dore, S., Kolb, T., Montes-Helu, M., Sullivan, B., Winslow, W., Hart, S., Kaye, J., Koch, G., & Hungate, B. (2008). Long-term impact of a stand-replacing fire on ecosystem CO_2 exchange of a Ponderosa pine forest. *Global Change Biology*, *14*, 1801–1820.

Dragoni, D., Schmid, H.P., Wayson, C.A., Potter, H., Grimmond, C.S.B., & Randolph, J.C. (2011). Evidence of increased net ecosystem productivity associated with a longer vegetated season in a deciduous forest in south-central Indiana, USA. *Global Change Biology*, *17*, 886–897.

Duan, Q., Gupta, V.K., & Sorooshian, S. (1993). Shuffled complex evolution approach for effective and efficient global minimization. *Journal of Optimization Theory and Applications*, *76*, 501–521.

Duan, Q.Y., Sorooshian, S., & Gupta, V. (1992). Effective and efficient global optimization for conceptual rainfall-runoff models. *Water Resources Research*, *28*, 1015–1031.

Fischer, M.L., Billesbach, D.P., Berry, J.A., Riley, W.J., & Torn, M.S. (2007). Spatiotemporal variations in growing season exchanges of CO_2, H_2O, and sensible heat in agricultural fields of the Southern Great Plains. *Earth Interactions*, *11*, 1–21.

Fisher, J.I., & Mustard, J.F. (2007). Cross-scalar satellite phenology from ground, Landsat, and MODIS data. *Remote Sensing of Environment*, *109*, 261–273.

Fisher, J.I., Richardson, A.D., & Mustard, J.F. (2007). Phenology model from surface meteorology does not capture satellite-based greenup estimations. *Global Change Biology*, *13*, 707–721.

Friedl, M.A., Gray, J.M., Melaas, E.K., Richardson, A.D., Hufkens, K., Keenan, T.F., Bailey, A., & O'Keefe, J. (2014). A tale of two springs: Using recent climate anomalies to characterize the sensitivity of temperate forest phenology to climate change. *Environmental Research Letters*, *9*, 054006.

Friedl, M.A., McIver, D.K., Hodges, J.C.F., Zhang, X.Y., Muchoney, D., Strahler, A.H., Woodcock, C.E., Gopal, S., Schneider, A., Cooper, A., Baccini, A., Gao, F., & Schaaf, C. (2002). Global land cover mapping from MODIS: Algorithms and early results. *Remote Sensing of Environment*, *83*, 287–302.

Friedl, M.A., Sulla-Menashe, D., Tan, B., Schneider, A., Ramankutty, N., Sibley, A., & Huang, X. (2010). MODIS Collection 5 global land cover: Algorithm refinements and characterization of new datasets. *Remote Sensing of Environment*, *114*, 168–182.

Ganguly, S., Friedl, M.A., Tan, B., Zhang, X., & Verma, M. (2010). Land surface phenology from MODIS: Characterization of the Collection 5 global land cover dynamics product. *Remote Sensing of Environment*, *114*, 1805–1816.

Gilmanov, T.G., Tieszen, L.L., Wylie, B.K., Flanagan, L.B., Frank, A.B., Haferkamp, M.R., Meyers, T.P., & Morgan, J.A. (2005). Integration of CO_2 flux and remotely-sensed data for primary production and ecosystem respiration analyses in the Northern Great Plains: Potential for quantitative spatial extrapolation. *Global Ecology and Biogeography*, *14*, 271–292.

Hanninen, H., & Kramer, K. (2007). A framework for modelling the annual cycle of trees in boreal and temperate regions. *Silva Fennica*, *41*, 167–205.

Hastings, D.A., & Dunbar, P. (1998). Development & assessment of the Global Land One-km Base Elevation digital elevation model (GLOBE). *Group*, *4*.

Heumann, B.W., Seaquist, J., Eklundh, L., & Jönsson, P. (2007). AVHRR derived phenological change in the Sahel and Soudan, Africa, 1982–2005. *Remote Sensing of Environment*, *108*, 385–392.

Huete, A., Didan, K., Miura, T., Rodriguez, E.P., Gao, X., & Ferreira, L.G. (2002). Overview of the radiometric and biophysical performance of the MODIS vegetation indices. *Remote Sensing of Environment*, *83*, 195–213.

Hufkens, K., Friedl, M., Sonnentag, O., Braswell, B.H., Milliman, T., & Richardson, A.D. (2012). Linking near-surface and satellite remote sensing measurements of deciduous broadleaf forest phenology. *Remote Sensing of Environment*, *117*, 307–321.

Jarvis, P.G., & McNaughton, K. (1986). Stomatal control of transpiration: Scaling up from leaf to region. *Advances in Ecological Research*, *15*, 1–49.

Jeong, S.J., Medvigy, D., Shevliakova, E., & Malyshev, S. (2012). Uncertainties in terrestrial carbon budgets related to spring phenology. *Journal of Geophysical Research, Biogeosciences*, *117*, G01030.

Ji, L., & Peters, A.J. (2004). A spatial regression procedure for evaluating the relationship between AVHRR-NDVI and climate in the northern Great Plains. *International Journal of Remote Sensing*, *25*, 297–311.

Jin, Z.N., Zhuang, Q.L., He, J.S., Luo, T.X., & Shi, Y. (2013). Phenology shift from 1989 to 2008 on the Tibetan Plateau: An analysis with a process-based soil physical model and remote sensing data. *Climatic Change*, *119*, 435–449.

Jolly, W.M., Nemani, R., & Running, S.W. (2005). A generalized, bioclimatic index to predict foliar phenology in response to climate. *Global Change Biology*, *11*, 619–632.

Jönsson, P., & Eklundh, L. (2004). TIMESAT—A program for analyzing time-series of satellite sensor data. *Computers & Geosciences*, *30*, 833–845.

Julien, Y., & Sobrino, J.A. (2009). Global land surface phenology trends from GIMMS database. *International Journal of Remote Sensing*, *30*, 3495–3513.

Justice, C., Townshend, J., Vermote, E., Masuoka, E., Wolfe, R., Saleous, N., Roy, D., & Morisette, J. (2002). An overview of MODIS Land data processing and product status. *Remote Sensing of Environment*, *83*, 3–15.

Kaduk, J.D., & Los, S.O. (2011). Predicting the time of green up in temperate and boreal biomes. *Climatic Change*, *107*, 277–304.

Kalfas, J.L., Xiao, X., Vanegas, D.X., Verma, S.B., & Suyker, A.E. (2011). Modeling gross primary production of irrigated and rain-fed maize using MODIS imagery and CO_2 flux tower data. *Agricultural and Forest Meteorology*, *151*, 1514–1528.

Koerner, C., & Basler, D. (2010). Phenology under global warming. *Science*, *327*, 1461–1462.

Please cite this article as: Xin, Q., et al., Modeling grassland spring onset across the Western United States using climate variables and MODIS-derived phenology metrics, *Remote Sensing of Environment* (2015), http://dx.doi.org/10.1016/j.rse.2015.02.003

Koster, R.D., & Suarez, M.J. (1992). Modeling the land surface boundary in climate models as a composite of independent vegetation stands. *Journal of Geophysical Research: Atmospheres*, *97*, 2697–2715.

Kucharik, C.J., Barford, C.C., El Maayar, M., Wofsy, S.C., Monson, R.K., & Baldocchi, D.D. (2006). A multiyear evaluation of a Dynamic Global Vegetation Model at three AmeriFlux forest sites: Vegetation structure, phenology, soil temperature, and CO_2 and H_2O vapor exchange. *Ecological Modelling*, *196*, 1–31.

Lammertsma, E.I., de Boer, H.J., Dekker, S.C., Dilcher, D.L., Lotter, A.F., & Wagner-Cremer, F. (2011). Global CO_2 rise leads to reduced maximum stomatal conductance in Florida vegetation. *Proceedings of the National Academy of Sciences*, *108*, 4035–4040.

Leuning, R. (1995). A critical appraisal of a combined stomatal-photosynthesis model for C3 plants. *Plant, Cell & Environment*, *18*, 339–355.

Levis, S., & Bonan, G.B. (2004). Simulating springtime temperature patterns in the community atmosphere model coupled to the community land model using prognostic leaf area. *Journal of Climate*, *17*, 4531–4540.

Liang, X., Lettenmaier, D.P., & Wood, E.F. (1996). One-dimensional statistical dynamic representation of subgrid spatial variability of precipitation in the two-layer variable infiltration capacity model. *Journal of Geophysical Research, [Atmospheres]*, *101*, 21403–21422.

Liu, H., Tian, F., Hu, H., Hu, H., & Sivapalan, M. (2013). Soil moisture controls on patterns of grass green-up in Inner Mongolia: An index based approach. *Hydrology and Earth System Sciences*, *17*, 805–815.

Lobell, D.B., Roberts, M.J., Schlenker, W., Braun, N., Little, B.B., Rejesus, R.M., & Hammer, G.L. (2014). Greater sensitivity to drought accompanies maize yield increase in the U.S. Midwest. *Science*, *344*, 516–519.

Lotsch, A., Friedl, M.A., Anderson, B.T., & Tucker, C.J. (2003). Coupled vegetation–precipitation variability observed from satellite and climate records. *Geophysical Research Letters*, *30*, 1774.

Luo, L., Robock, A., Mitchell, K.E., Houser, P.R., Wood, E.F., Schaake, J.C., Lohmann, D., Cosgrove, B., Wen, F., & Sheffield, J. (2003). Validation of the North American Land Data Assimilation System (NLDAS) retrospective forcing over the southern Great Plains. *Journal of Geophysical Research, [Atmospheres], 1984–2012*, 108.

Maurer, E., Wood, A., Adam, J., Lettenmaier, D., & Nijssen, B. (2002). A long-term hydrologically based dataset of land surface fluxes and States for the Conterminous United States. *Journal of Climate*, *15*, 3237–3251.

Melaas, E.K., Friedl, M.A., & Zhu, Z. (2013). Detecting interannual variation in deciduous broadleaf forest phenology using Landsat TM/ETM+ data. *Remote Sensing of Environment*, *132*, 176–185.

Melaas, E.K., Richardson, A.D., Friedl, M.A., Dragoni, D., Gough, C.M., Herbst, M., Montagnani, L., & Moors, E. (2013). Using FLUXNET data to improve models of springtime vegetation activity onset in forest ecosystems. *Agricultural and Forest Meteorology*, *171*, 46–56.

Metropolis, N., Rosenbluth, A.W., Rosenbluth, M.N., Teller, A.H., & Teller, E. (1953). Equation of state calculations by fast computing machines. *The Journal of Chemical Physics*, *21*, 1087–1092.

Myneni, R.B., Hall, F.G., Sellers, P.J., & Marshak, A.L. (1995). The interpretation of spectral vegetation indexes. *IEEE Transactions on Geoscience and Remote Sensing*, *33*, 481–486.

Nijland, W., de Jong, R., de Jong, S.M., Wulder, M.A., Bater, C.W., & Coops, N.C. (2014). Monitoring plant condition and phenology using infrared sensitive consumer grade digital cameras. *Agricultural and Forest Meteorology*, *184*, 98–106.

Peng, S., Piao, S., Zeng, Z., Ciais, P., Zhou, L., Li, L.Z., Myneni, R.B., Yin, Y., & Zeng, H. (2014). Afforestation in China cools local land surface temperature. *Proceedings of the National Academy of Sciences*, *111*, 2915–2919.

Piao, S., Cui, M., Chen, A., Wang, X., Ciais, P., Liu, J., & Tang, Y. (2011). Altitude and temperature dependence of change in the spring vegetation green-up date from 1982 to 2006 in the Qinghai-Xizang Plateau. *Agricultural and Forest Meteorology*, *151*, 1599–1608.

Piao, S., Fang, J., Zhou, L., Ciais, P., & Zhu, B. (2006). Variations in satellite-derived phenology in China's temperate vegetation. *Global Change Biology*, *12*, 672–685.

Piao, S., Friedlingstein, P., Ciais, P., Viovy, N., & Demarty, J. (2007). Growing season extension and its impact on terrestrial carbon cycle in the Northern Hemisphere over the past 2 decades. *Global Biogeochemical Cycles*, *21*.

Richardson, A.D., Anderson, R.S., Arain, M.A., Barr, A.G., Bohrer, G., Chen, G.S., Chen, J.M., Ciais, P., Davis, K.J., Desai, A.R., Dietze, M.C., Dragoni, D., Garrity, S.R., Gough, C.M., Grant, R., Hollinger, D.Y., Margolis, H.A., McCaughey, H., Migliavacca, M., Monson, R.K., Munger, J.W., Poulter, B., Raczka, B.M., Ricciuto, D.M., Sahoo, A.K., Schaefer, K., Tian, H.Q., Vargas, R., Verbeeck, H., Xiao, J.F., & Xue, Y.K. (2012). Terrestrial biosphere models need better representation of vegetation phenology: Results from the North American Carbon Program Site Synthesis. *Global Change Biology*, *18*, 566–584.

Richardson, A.D., Bailey, A.S., Denny, E.G., Martin, C.W., & O'Keefe, J. (2006). Phenology of a northern hardwood forest canopy. *Global Change Biology*, *12*, 1174–1188.

Richardson, A.D., Black, T.A., Ciais, P., Delbart, N., Friedl, M.A., Gobron, N., Hollinger, D.Y., Kutsch, W.L., Longdoz, B., & Luyssaert, S. (2010). Influence of spring and autumn phenological transitions on forest ecosystem productivity. *Philosophical Transactions of the Royal Society, B: Biological Sciences*, *365*, 3227–3246.

Richardson, A.D., Keenan, T.F., Migliavacca, M., Ryu, Y., Sonnentag, O., & Toomey, M. (2013). Climate change, phenology, and phenological control of vegetation feedbacks to the climate system. *Agricultural and Forest Meteorology*, *169*, 156–173.

Roy, D., Jin, Y., Lewis, P., & Justice, C. (2005). Prototyping a global algorithm for systematic fire-affected area mapping using MODIS time series data. *Remote Sensing of Environment*, *97*, 137–162.

Schaake, J.C., Duan, Q., Koren, V., Mitchell, K.E., Houser, P.R., Wood, E.F., Robock, A., Lettenmaier, D.P., Lohmann, D., & Cosgrove, B. (2004). An intercomparison of soil moisture fields in the North American Land Data Assimilation System (NLDAS). *Journal of Geophysical Research, [Atmospheres], 1984–2012*, 109.

Scott, R.L. (2010). Using watershed water balance to evaluate the accuracy of eddy covariance evaporation measurements for three semiarid ecosystems. *Agricultural and Forest Meteorology*, *150*, 219–225.

Shen, M., Tang, Y., Chen, J., Zhu, X., & Zheng, Y. (2011). Influences of temperature and precipitation before the growing season on spring phenology in grasslands of the central and eastern Qinghai-Tibetan Plateau. *Agricultural and Forest Meteorology*, *151*, 1711–1722.

Tan, B., Morisette, J.T., Wolfe, R.E., Feng, G., Ederer, G.A., Nightingale, J., & Pedelty, J.A. (2011). An enhanced TIMESAT algorithm for estimating vegetation phenology metrics from MODIS data. *IEEE Journal of Selected Topics in Applied Earth Observations and Remote Sensing*, *4*, 361–371.

Tateishi, R., & Ebata, M. (2004). Analysis of phenological change patterns using 1982–2000 Advanced Very High Resolution Radiometer (AVHRR) data. *International Journal of Remote Sensing*, *25*, 2287–2300.

Thornton, P., Thornton, M., Mayer, B., Wilhelmi, N., Wei, Y., & Cook, R. (2012). *Daymet: Daily surface weather on a 1 km grid for North America, 1980–2008.* Oak Ridge, T, N: Oak Ridge National Laboratory Distributed Active Archive Center (doi, 10).

Wang, X., Piao, S., Ciais, P., Li, J., Friedlingstein, P., Koven, C., & Chen, A. (2011). Spring temperature change and its implication in the change of vegetation growth in North America from 1982 to 2006. *Proceedings of the National Academy of Sciences*, *108*, 1240–1245.

White, M.A., BEURS, D., Kirsten, M., Didan, K., Inouye, D.W., Richardson, A.D., Jensen, O.P., O'keefe, J., Zhang, G., & Nemani, R.R. (2009). Intercomparison, interpretation, and assessment of spring phenology in North America estimated from remote sensing for 1982–2006. *Global Change Biology*, *15*, 2335–2359.

White, M.A., Thornton, P.E., & Running, S.W. (1997). A continental phenology model for monitoring vegetation responses to interannual climatic variability. *Global Biogeochemical Cycles*, *11*, 217–234.

Willmott, C.J., Ackleson, S.G., Davis, R.E., Feddema, J.J., Klink, K.M., Legates, D.R., O'Donnell, J., & Rowe, C.M. (1985). Statistics for the evaluation and comparison of models. *Journal of Geophysical Research, Oceans*, *90*, 8995–9005.

Wu, C.Y., Gonsamo, A., Gough, C.M., Chen, J.M., & Xu, S.G. (2014). Modeling growing season phenology in North American forests using seasonal mean vegetation indices from MODIS. *Remote Sensing of Environment*, *147*, 79–88.

Wu, X., & Liu, H. (2013). Consistent shifts in spring vegetation green-up date across temperate biomes in China, 1982–2006. *Global Change Biology*, *19*, 870–880.

Xia, Y., Mitchell, K., Ek, M., Sheffield, J., Cosgrove, B., Wood, E., Luo, L., Alonge, C., Wei, H., & Meng, J. (2012). Continental-scale water and energy flux analysis and validation for the North American Land Data Assimilation System project phase 2 (NLDAS-2): 1. Intercomparison and application of model products. *Journal of Geophysical Research, [Atmospheres]*, *117*.

Xiao, J., Zhuang, Q., Law, B.E., Chen, J., Baldocchi, D.D., Cook, D.R., Oren, R., Richardson, A.D., Wharton, S., & Ma, S. (2010). A continuous measure of gross primary production for the conterminous United States derived from MODIS and AmeriFlux data. *Remote Sensing of Environment*, *114*, 576–591.

Xin, Q., Broich, M., Suyker, A.E., Yu, L., & Gong, P. (2015). Multi-scale evaluation of light use efficiency in MODIS gross primary productivity for croplands in the Midwestern United States. *Agricultural and Forest Meteorology*, *201*, 111–119.

Xin, Q., Olofsson, P., Zhu, Z., Tan, B., & Woodcock, C.E. (2013). Toward near real-time monitoring of forest disturbance by fusion of MODIS and Landsat data. *Remote Sensing of Environment*, *135*, 234–247.

Xin, Q., Woodcock, C.E., Liu, J., Tan, B., Melloh, R.A., & Davis, R.E. (2012). View angle effects on MODIS snow mapping in forests. *Remote Sensing of Environment*, *118*, 50–59.

Yang, X., Mustard, J.F., Tang, J., & Xu, H. (2012). Regional-scale phenology modeling based on meteorological records and remote sensing observations. *Journal of Geophysical Research, Biogeosciences, 2005–2012*, 117.

Yu, F., Price, K.P., Ellis, J., & Shi, P. (2003). Response of seasonal vegetation development to climatic variations in eastern central Asia. *Remote Sensing of Environment*, *87*, 42–54.

Zhang, X., Friedl, M.A., Schaaf, C.B., Strahler, A.H., Hodges, J.C., Gao, F., Reed, B.C., & Huete, A. (2003). Monitoring vegetation phenology using MODIS. *Remote Sensing of Environment*, *84*, 471–475.

Zhang, G., Zhang, Y., Dong, J., & Xiao, X. (2013). Green-up dates in the Tibetan Plateau have continuously advanced from 1982 to 2011. *Proceedings of the National Academy of Sciences*, *110*, 4309–4314.

Zhu, Z., Bi, J., Pan, Y., Ganguly, S., Anav, A., Xu, L., Samanta, A., Piao, S., Nemani, R.R., & Myneni, R.B. (2013). Global data sets of vegetation leaf area index (LAI) 3g and Fraction of Photosynthetically Active Radiation (FPAR) 3g derived from Global Inventory Modeling and Mapping Studies (GIMMS) Normalized Difference Vegetation Index (NDVI3g) for the period 1981 to 2011. *Remote Sensing*, *5*, 927–948.

Please cite this article as: Xin, Q., et al., Modeling grassland spring onset across the Western United States using climate variables and MODIS-derived phenology metrics, *Remote Sensing of Environment* (2015), http://dx.doi.org/10.1016/j.rse.2015.02.003